Geochemistry, Geophysics, Geosystems®

RESEARCH ARTICLE
10.1029/2024GC011822

Trace Element Emissions Vary With Lava Flow Age and Thermal Evolution During the Fagradalsfjall 2021–2023 Eruptions, Iceland

L. Wainman[1], E. Ilyinskaya[1], M. Pfeffer[2], C. Mandon[3], E. Bali[3], B. A. Edwards[4,5], B. I. Kleine-Marshall[6], S. R. Gudjonsdottir[3], A. Cotterill[7], S. W. Scott[3], P. Wieser[8], A. Stefánsson[3], E. J. Nicholson[7,9], J. Sepulveda-Araya[1], S. J. Hammond[10], B. E. Kunz[10], F. Jenner[10], J. R. Gunnarsson[3], A. Aiuppa[11], M. Burton[12], and T. A. Mather[13]

[1]School of Earth and Environment, University of Leeds, Leeds, UK, [2]Icelandic Meteorological Office, Reykjavík, Iceland, [3]Institute of Earth Sciences, University of Iceland, Reykjavik, Iceland, [4]Centre for Earth Observation Science, Department of Environment and Geography, University of Manitoba, Winnipeg, MB, Canada, [5]Geological Survey of Canada, Natural Resources Canada, Ottawa, ON, Canada, [6]GeoZentrum Nordbayern, Friedrich-Alexander University Erlangen-Nuremberg, Erlangen, Germany, [7]Department of Earth Sciences, University College London, London, UK, [8]Earth and Planetary Science, UC Berkeley, Berkeley, CA, USA, [9]School of Science, University of Waikato, Hamilton, New Zealand, [10]School of Environment, Earth and Ecosystem Sciences, The Open University, Milton Keynes, UK, [11]Dipartimento di Scienze della Terra e del Mare, Università degli Studi di Palermo, Palermo, Italy, [12]Department of Earth and Environmental Sciences, University of Manchester, Manchester, UK, [13]Department of Earth Sciences, University of Oxford, Oxford, UK

Key Points:

- Particulate matter and gases were measured in lava flow emissions at increasing distances from the crater (increasing lava ages) as well as above a stagnant lava pond at the Fagradalsfjall 2021–2023 eruptions
- Thermochemical modeling suggests that speciation is a key control on the down-flow fractionation in trace element outgassing from cooling lavas
- Sulfur-complexing element (Se, Te, As) emissions decreased most rapidly down-flow whilst some chloride-complexed (Cu, Rb, Cs) elements became more abundant relative to at-crater emissions

Supporting Information:

Supporting Information may be found in the online version of this article.

Correspondence to:

L. Wainman,
eelrw@leeds.ac.uk

Citation:

Wainman, L., Ilyinskaya, E., Pfeffer, M., Mandon, C., Bali, E., Edwards, B. A., et al. (2024). Trace element emissions vary with lava flow age and thermal evolution during the Fagradalsfjall 2021–2023 eruptions, Iceland. *Geochemistry, Geophysics, Geosystems*, *25*, e2024GC011822. https://doi.org/10.1029/2024GC011822

Received 12 AUG 2024
Accepted 26 OCT 2024

Author Contributions:

Conceptualization: E. Ilyinskaya
Formal analysis: L. Wainman, E. Ilyinskaya, E. Bali, S. J. Hammond, B. E. Kunz, F. Jenner, J. R. Gunnarsson
Funding acquisition: E. Bali, T. A. Mather
Investigation: L. Wainman, E. Ilyinskaya, M. Pfeffer, C. Mandon, E. Bali, B. A. Edwards, B. I. Kleine-Marshall,

Abstract Basaltic fissure eruptions emit volatile and environmentally reactive gases and particulate matter (PM) into the lower troposphere (e.g., SO_2, HCl, and HF in the gas phase; Se, As, Pb as complexes in the PM phase). Lava flows from fissure eruptions can be spatially extensive, but the composition and fluxes of their emissions are poorly characterized compared to those from main vent(s). Using uncrewed aircraft systems-mounted (drone) samplers and ground-based remote Fourier Transform Infrared Spectroscopy, we investigated the down-flow compositional evolution of emissions from active lava flows during the Fagradalsfjall 2021–2023 eruptions. The calculated fluxes of volatile trace metals from lava flows are considerable relative to both main vent degassing and anthropogenic fluxes in Iceland. We demonstrate a fractionation in major gas emissions with decreasing S/halogen ratio down-flow. This S-Cl fractionation is reflected in the trace element degassing profile, where the abundance of predominantly sulfur-complexing elements (e.g., Se, Te, As, Pb) decreases more rapidly in down-flow emissions relative to elements complexing as chlorides (e.g., Cu, Rb, Cs), oxides (e.g., La, Ce) and hydroxides (e.g., Fe, Mg, Al, Ti). Using thermochemical modeling, we explain this relationship through temperature and composition dependent element speciation as the lava flow ages and cools. As a result, some chloride-complexing elements (such as Cu) become relatively more abundant in emissions further down-flow, compared to emissions from the main vent or more proximal lava flows. This variability in down-flow element fluxes suggests that the output of metals to the environment may change depending on lava flow age and thermal evolution.

Plain Language Summary Lava flows, such as those formed during the recent eruptions in Iceland (2021–2023), emit gases, particles and droplets to the atmosphere. These include an array of different metals, some of which may be harmful to the environment and human health. In this study, we use drone-mounted equipment and a remote-sensing spectrometer to collect samples and the measure gases and particles above lava flows at increasing distances from the vent. Some elements that predominantly bond with sulfur tend to diminish in abundance as the lava flow ages, while those elements that predominantly bond with chloride increase in abundance with increasing distance from the vent. By modeling how elements preferentially bond together at different temperatures, we can explain how different elements behave when emitted from increasingly colder lava flows. Overall, the quantity of metals emitted from lava flows during the Fagradalsfjall eruption is equal to or greater than emissions from human-related activity in Iceland during 2021.

1. Introduction

Volcanic emissions from effusive basaltic fissure eruptions consist of major gases (H_2O, SO_2, H_2S, CO_2, HCl, HF) and particulate matter (PM), including an array of metal and metalloid trace elements (Symonds et al., 1987;

S. R. Gudjonsdottir, A. Cotterill, S. W. Scott, A. Stefánsson, E. J. Nicholson, J. Sepulveda-Araya, A. Aiuppa, M. Burton, T. A. Mather
Methodology: L. Wainman, E. Ilyinskaya, M. Pfeffer, C. Mandon, E. Bali, S. W. Scott, A. Stefánsson, E. J. Nicholson, S. J. Hammond, B. E. Kunz, F. Jenner, A. Aiuppa, M. Burton
Resources: L. Wainman, E. Ilyinskaya, E. J. Nicholson, M. Burton, T. A. Mather
Supervision: E. Ilyinskaya, M. Pfeffer
Visualization: L. Wainman, E. Ilyinskaya
Writing – original draft: L. Wainman, E. Ilyinskaya, M. Pfeffer
Writing – review & editing: L. Wainman, E. Ilyinskaya, M. Pfeffer, C. Mandon, E. Bali, B. A. Edwards, B. I. Kleine-Marshall, S. R. Gudjonsdottir, A. Cotterill, S. W. Scott, E. J. Nicholson, J. Sepulveda-Araya, S. J. Hammond, B. E. Kunz, F. Jenner, A. Aiuppa, M. Burton, T. A. Mather

Zoller et al., 1983). Some of these elements, such as As, Cd, Cr, Pb, Se, Tl, and W, are classified as "metal pollutants" (World Health Organization, 2007) and thus, are both an environmental and air quality hazard for exposed communities (Stewart et al., 2021). During intense and prolonged activity, the eruptive outgassing of trace metal and metalloid elements can be comparable to anthropogenic emission fluxes from entire regions and countries (Ilyinskaya et al., 2021). Metal and metalloid elements are released during magma degassing directly into the atmosphere, either as free gases, or more commonly, complexed with major gas species to form oxides, halides (such as chlorides or fluorides), sulfides, sulfates, hydrides, or hydroxides (Mandon et al., 2019; Moune et al., 2010; Symonds et al., 1992; Zelenski et al., 2021). Upon outgassing at the air interface, metal and metalloid bearing gases are rapidly partitioned into a particulate phase (defined in this paper as particulate matter (PM)) either via desublimation (gas-to-particle conversion), droplet condensation (Symonds et al., 1987), or scavenging of metal and metalloid elements by aerosols and ash (Moune et al., 2006). The composition and total emission flux of metal and metalloid elements are controlled by several factors, including melt composition, oxygen fugacity (fO_2), and the thermodynamic properties of metal/metalloid-containing compounds (Churakov et al., 2000; Symonds et al., 1987; Symonds & Reed, 1993; Williams-Jones & Heinrich, 2005). Melt composition is a primary control both on the concentrations of metals themselves, as well as on the availability of key ligand-forming elements (S, O, H, Cl, F), which are critical to metal speciation and emission (Hinkley et al., 1994; Symonds et al., 1992; Zelenski et al., 2021). Gas emissions from hotspot basaltic eruptions such as from Kīlauea (Hawai'i) and Holuhraun 2014–2015 (Iceland) are generally lower in Cl relative to eruptions in arc settings, reflecting the more limited availability of the Cl ligand due to the absence of a recycled slab component (Allard et al., 2016; Edmonds et al., 2018; Gauthier et al., 2016; Mandon et al., 2019; Mather et al., 2012). Hotspot settings are generally associated with lower metal fluxes and a higher relative abundance of sulfur-complexing elements such as Se, Te, and Cd, although few studies have investigated this in the context of rift-dominated systems such as the Reykjanes Peninsula (Edmonds et al., 2018; Zelenski et al., 2013).

Degassing from the main volcanic vent(s) has been the primary focus of previous investigations (Ilyinskaya et al., 2017; Mandon et al., 2019; Mason et al., 2021; Mather et al., 2012), and yet basaltic eruptions also generate extensive lava flows, which can be an additional source of gas and PM emissions (e.g., Thordarson & Self, 2003) Toutain et al. (1990) found that down-flow sublimate mineral assemblages at Piton de la Fournaise volcano were dominated by chlorides and fluorides but lacked sulfides, sulfates, or oxides, which were most likely degassed closer to the vent. They did not link this to individual trace element behavior, however, and instead suggested that the distribution of elements depends on temperature and element volatility, with the more volatile elements such as Rb, Cs, Se, Pb and Tl being associated with deposits from lower-temperature flows. Previous approaches have defined metal volatility using either an emanation coefficient (ε_x) describing the extent to which an element is released in the gas phase (Edmonds et al., 2018; Pennisi et al., 1988) or an enrichment factor (EF) describing the degree to which an element is enriched in the volcanic gas and non-silicate aerosol phase relative to silicate material (Aiuppa et al., 2003; Mandon et al., 2019; Moune et al., 2010). Moderate to highly volatile elements are defined as having $\varepsilon_x > 0.05\%$ (Rubin, 1997) and include elements such as Te, Se, Cd, Pb, As, Ag, and Sn, whilst more refractory elements include those such as Fe, Ce, La, Ca, and Mg, which have $\varepsilon_x < 0.001\%$. Recent advances in sampling and analytical approaches have prompted renewed study of down-flow degassing evolution, with analysis of individual trace element evolution, and simultaneous gas measurements at increasing distances down-flow. Quantification of the magnitude of metal and metalloid emissions from lava flows, relative to main vent degassing and anthropogenic emissions, is also important for understanding their relative contribution to potential tropospheric air quality and environmental hazards. This knowledge is particularly important if lava flows extend kilometers away from the main eruptive vent towards population centers, exacerbating the likelihood of ground-based exposure to volcanic pollutants such as SO_2, PM less than 2.5 μm ($PM_{2.5}$), PM less than 10 μm (PM_{10}) and metal and metalloid elements (e.g., Pb, As, Cd) emitted from lava flows.

In this study, we used filter packs mounted on uncrewed aircraft systems (UAS) and Fourier Transform Infrared Spectroscopy (FTIR) to investigate the at-crater and down-flow emission of gases and trace elements during the 2021–2023 Fagradalsfjall eruptions on the Reykjanes Peninsula. Combined with equilibrium thermochemical modeling, we demonstrate that element speciation, which shows a dependence on lava temperature, is a key control on degassing behavior and down-flow fractionation in trace element emissions. Finally, we quantify the respective fluxes of volatile trace elements from at-crater and lava flow sources, showing that they both equal or exceed Icelandic anthropogenic emissions in 2021 during periods of active eruptive activity.

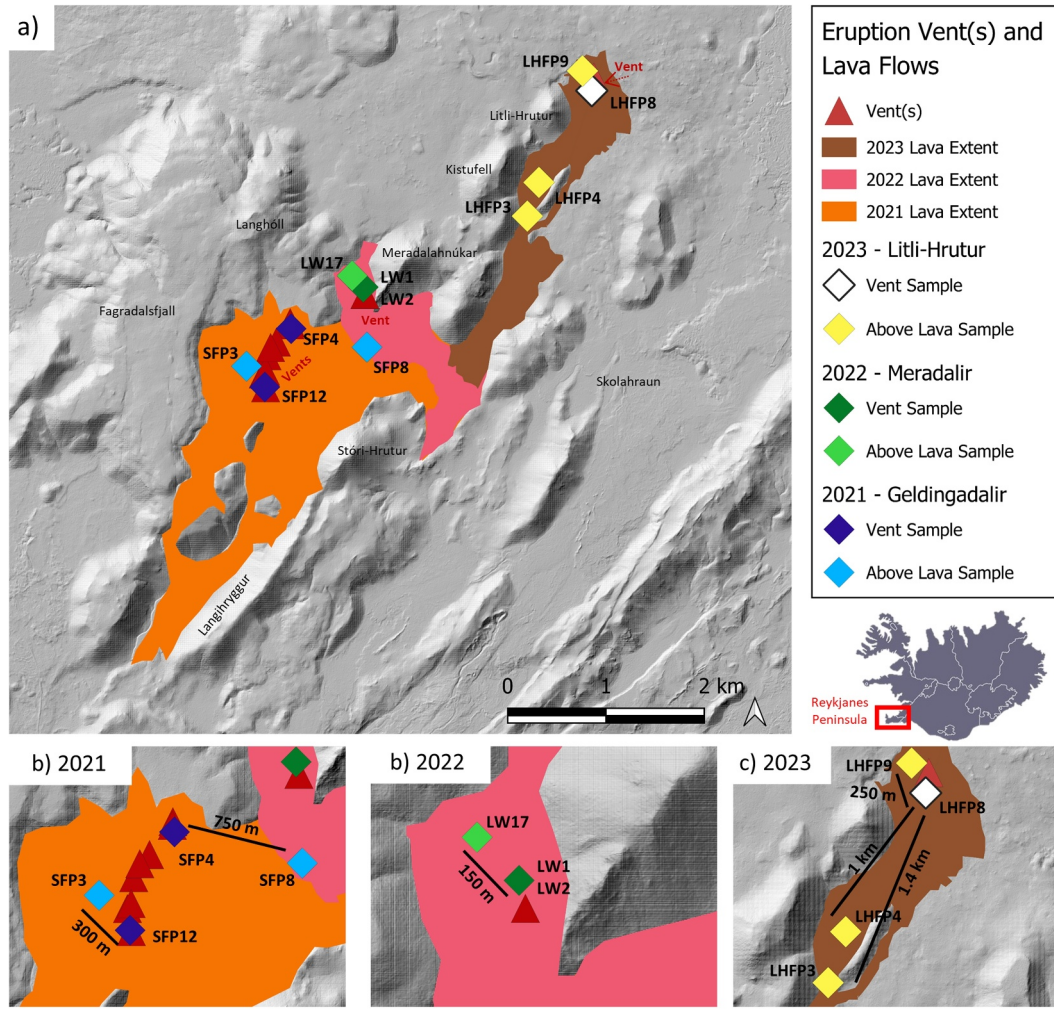

Figure 1. Map of sampling locations. (a) Overview of lava flow extent for the three eruptions included in this study, red triangles show the locations of active vents. Diamonds show filter pack sampling locations, with darker colors showing at-vent samples and lighter colors showing samples collected above actively degassing lava flows. (b) Fagradalsfjall 2021—SFP3, SFP4, SFP8, and SFP12 were collected on separate days with lava samples (SFP3 and SFP8) at 300 and 750 m from their concurrently active vents (SFP4 and SFP12, respectively). (c) Meradalir 2022—LW17 was collected 150 m from the vent above a perched lava pond. LW1 and LW2 were both collected above the main active vent. (d) Litli-Hrútur 2023—LHFP3 and LHFP4 were collected on the same day at 1.4 and 1 km from the vent (LFP8), respectively, with LHFP9 collected subsequently at 250 m from the vent.

2. Geological Context

2.1. The Fagradalsfjall Eruptions 2021–2023

The three eruptions included in this study (2021 Geldingadalir, 2022 Meradalir and 2023 Litli Hrútur) occurred within the Fagradalsfjall volcanic system, which is one of six volcanic systems in the Reykjanes Volcanic Zone on the Reykjanes Peninsula (See Figure 1 and Einarsson & Sigurgeirsson, 2019). Prior to the eruption in 2021, the Fagradalsfjall system had been dormant for 6,000 years, while the wider peninsula had 800 years of quiescence. The 2022 and 2023 eruptions migrated progressively NE compared to the location of the 2021 eruption, although all fissures had a similar NE-SW strike and were located within ~5 km of each other.

2.1.1. Geldingadalir 2021 Eruption

Following a 14-month period of seismic unrest (Barsotti et al., 2023), the 2021 Fagradalsfjall eruption began on the 19th March (Halldórsson et al., 2022; Sigmundsson et al., 2022). The eruption continued for 6 months and

progressed through four stages of activity (stages defined by Barsotti et al., 2023; Pedersen et al., 2022). The earliest stage (Phase I: 19th March–5th April) was characterized by effusive activity from a single vent, followed by the opening of additional vents (including vents 2, 3, and 5 from which gas emissions were measured with FTIR, see Section 3.3 below) during Phase II (5th April–27th April). The composition of the lava changed significantly during the first 50 days of the eruption (between Phase I and Phase II) from a depleted low K_2O/TiO_2 composition to one that was more enriched, with a higher K_2O/TiO_2 ratio (Halldórsson et al., 2022). During Phase III (27th April–28th June) activity was again concentrated to a single vent before the intensity of activity decreased during Phase IV (28 June–18 September) and lava effusion from the main vent became cyclical. All phases of activity were associated with the emission of a plume of gas (Pfeffer et al., 2024) and PM from the main vent(s) as well as lava flows extending several kilometers from the main crater(s). The mean lava thickness for the eruption exceeded 30 m, covering 4.8 km^2 with a bulk volume of $150 \pm 3 \times 10^6$ m^3 (Pedersen et al., 2022). The mean bulk effusion rate varied between phases of the eruption, ranging from 1 to 8 m^3/s in March–April and increasing to 9–13 m^3/s in May–September (Pedersen et al., 2022). Volcanic plume samples presented in this work were collected on 23rd March 2021 (SFP3 and SFP4, Phase I) and 6th April 2021 (SFP8 and SFP12), Phase II). Figure 1 shows lava flow and sample location maps.

2.1.2. Meradalir 2022 Eruption

On 3rd August 2022 an eruption began at Meradalir, ∼1 km to the NE of the previous eruption site on the Reykjanes Peninsula. After the initial fissure opening, activity became localized to a single vent, which was active until 21st August 2022. The effusion rate was initially 32 m^3/s during the first hours of the eruption, then waned to an average of 11 m^3/s between 4th and 13th August and decreased further to 3–4 m^3/s between 13th and 15th August (Gunnarson et al., 2023). Lava flows between 5 and 15 m thick extended up to 2 km into the Meradalir valley, although they were less laterally extensive than flows formed in the 2021 eruption, with a perched lava pond of 20–40 m thickness forming around the active crater. One lava flow sample was collected above a visibly degassing vent on the edge of the lava pond on 19th August 2022 (LW17) and two above vent samples were collected (LW1 and LW2) on 16th August 2022—see Figure 1 and Table 1.

2.1.3. Litli-Hrútur 2023 Eruption

On 10th July 2023 an eruption started near Litli-Hrútur ∼2 km to the NE of the 2022 Meradalir eruption and continued until 5th August 2023. Multiple eruption fissures stretched over 1 km with an initial effusion rate of up to 50 m^3/s during the first day of the eruption (Global Volcanism Program, 2023). The fissure quickly reduced to form a single active cone with an average effusion rate of 9–13 m^3/s for the first several weeks of the eruption, before decreasing to 3–4 m^3/s by early August (Global Volcanism Program, 2023). Lava flowed generally southwards, laterally extending toward the lava from the Meradalir 2022 eruption, although several crater rim collapses led to lava flowing toward the north and west of the crater. Extensive wildfires were also generated where lava flows ignited moss that covered much of the landscape in this region. Three samples were collected above laterally extending lava flows on 13th July 2023 (LHFP3 and LHFP4) and 19th July 2023 (LHFP9) and above the active vent on 19th July 2023 (LHFP8); see also Figure 1 and Table 1. Samples in 2023 were collected upwind of nearby wildfires to minimize contamination of the filters by wildfire pollution.

3. Sampling and Analytical Methods

3.1. Filter Pack Sampling

Filter packs mounted on UAS (DJI Matrice 600 Pro in 2021, DJI Matrice 300 RTK in 2022 and 2023, see Supporting Information S1 for full drone set up) were used to collect in situ samples of gases and aerosol PM above degassing lava flows. Total sampling duration ranged from 15 to 70 min, although due to UAS battery life limitations, most samples were the cumulation of multiple flights to the same location (see Table 1). The UAS hovered as close as vertically possible (∼20–60 m) above the lava surface where lava outgassing was visible, limited by the heat from the lava flows. Samples were collected at a range of distances from the main vent, from 200 m to 1.4 km down-flow across the three sampling years. A Multi-GAS instrument from the University of Palermo (Aiuppa et al., 2005; Liu et al., 2020, the same unit type used in Burton et al., 2023) was co-located on the drone for simultaneous time-series measurements of SO_2 concentrations (time resolution 1 Hz). The Multi-GAS

Table 1
Overview of Sampling Measurements Collected in This Study

Filter packs							
Sample ID	Sampling date	Lava flow style	Distance from vent (m)	Plume volume pumped (L)	Filter pack set up	Number of flights	On-board MultiGAS
SFP3	23/03/2021	Lava (Linear)	300	149	3G + PM	2	Yes
SFP4	23/03/2021	At-crater	<100	117	3G + PM	1	Yes
SFP8	06/04/2021	Lava (Linear)	800	171	PM Only	3	Yes
SFP12	13/04/2021	At-crater	<100	493	PM Only	4	Yes
LW1	16/08/2022	At-crater	<100	830	3G + PM	3	Yes
LW2	16/08/2022	At-crater	<100	176	3G + PM	1	Yes
LW17	21/08/2022	Lava (Ponded)	150	248	PM Only	1	Yes
LHFP3	13/07/2023	Lava (Linear)	1,400	527[a]	3G + PM	3	No
LHFP4	13/07/2023	Lava (Linear)	1,000	548[a]	PM Only	3	No
LHFP8	19/07/2023	At-crater	<100	514	PM Only	2	Yes
LHFP9	19/07/2023	Lava (Linear)	250	52.3	3G + PM	2	Yes

FTIR				
Source name	Date	Measurement Type	Description	Range from source (m)
5A	4/14/2021	At-crater	5A center top vent	154 ± 3
5A	4/14/2021	At-crater	5A right top vent	152 ± 3
5B	4/14/2021	At-crater	5B left wall vent	155 ± 2
5B-L	4/14/2021	Lava (Linear)	5B bottom where lava running out	143 ± 3
5A-L	4/14/2021	Lava (Linear)	5A main outflow	129 ± 3
5AB-M	4/14/2021	Lava (Linear)	5A and 5B merging lava rivers	103 ± 3
3-L	4/14/2021	Lava (Linear)	top of new lava river left side of 3	161 ± 4
B	3/23/2021	At-crater	main vent intermittent lava spatters	187 ± 11
A	3/23/2021	At-crater	2nd vent	175 ± 4
D	3/23/2021	Lava (Linear)	fast flowing lava channel end margin	280 ± 12
E	3/23/2021	Lava (Linear)	high speed lava channel	195 ± 2
C	3/23/2021	Lava (Linear)	lava flow right side of cone	277 ± 8

Note. Sheet S2 in Data Set S1 has an expanded version of filter pack sample metadata and Sheet S6 in Data Set S1 has expanded FTIR metadata. Raw MultiGAS files are included in Sheets S14–16 in Data Set S1. [a]Simultaneous Multi-GAS data was not collected on two flights in 2023; hence, no in-plume correction has been applied. Plume volume and plume sample duration therefore refer to total volume and total sample duration. PM Only = single PTFE filter loading in filter pack. 3G + PM = PTFE filter on first stage with three gas filters on subsequent stages.

contains SO_2 and H_2S electrochemical sensors (T3ST/F-TD2G-1A and T3H-TC4E-1A; both City Technology) and is calibrated for 0 to 200 ppmv and 0 to 50 ppmv, respectively—see Liu et al. (2020).

Mounted filter packs consisting of four stages were used in two different configurations: either containing just one filter for PM collection (PM Filter specifications: Whatman™ WTP polytetrafluoroethylene (PTFE) 47-mm diameter, pore size 1.0 μm) or with an additional 3 filters loaded behind the first PM filter for gas collection (Gas Filter Specifications: Whatman™ Quantitative Filter Papers, Ashless, Grade 41, 55-mm diameter (2021) and 47-mm diameter (2022), Millipore 47-mm diameter absorbent pads (2023)). The filters for gas collection were impregnated (5% K_2CO_3 + 1% glycerol in 2021, 5% KOH + 1% glycerol in 2022 and 2023) shortly prior to use (Ilyinskaya et al., 2017; Mason et al., 2021). Base treatment of gas filters allows for the capture of acidic gases such as SO_2, HCl, and HF by reaction and conversion to their anions SO_4^{2-}, SO_3^{2-}, Cl^-, and F^-. Gas filters were considered saturated if >10% of total SO_4^{2-} was present on the final gas filter stage (as defined by Mason et al., 2021). All gas filters collected in 2021 were saturated, and thus we decided to use KOH rather than K_2CO_3 impregnation for the gas filters in 2022 and 2023. Gas filters in 2022 and 2023 did not saturate despite being exposed to comparable SO_2 concentrations across similar flight durations. Airflow through the filter pack was

generated using an SKC Leland Legacy pump also mounted on the UAS (see Table 1 and Data Set S1 for individual sample flow rates). The flow rate was set to the highest value that the pump was able to sustain (6–13 L/min). The highest sustained flow rate varied according to which filter set up was used (i.e., 1 or 4 filters loaded) and was also sensitive to the curvature of the connective tubing between the pump and filter when mounting the equipment on the drone. Immediately after sampling, filter packs were sealed using Parafilm to prevent particle loss and contamination during transport.

Time-averaged in-plume SO_2 concentrations were calculated using the co-collected Multi-GAS SO_2 timeseries, excluding data <0.5 ppmv (the baseline between in-plume peaks in SO_2) within the known flight-time window. Mason et al. (2021) and Edwards et al. (2024) use background thresholds of 1 ppmv and 1.3 ppmv, respectively. Using alternative baselines of 0 and 1 ppmv resulted in a difference of less than 1% in our corrected in-plume flight times. The time averaged SO_2 concentrations should be viewed as minimum values as some in-plume measurements were made when SO_2 concentrations were above the maximum detection limit of the sensor (saturation occurred at ∼220 ppmv, % of time above Multi-GAS saturation recorded in Data Set S1). The total time filter packs spent inside the aerosol plume (defined as $SO_2 > 0.5$ ppmv) was used to correct for the total plume volume sampled by the filter packs.

3.2. Extraction and Compositional Analysis

The samples were handled in a class-10000 clean lab environment at the Institute of Earth Sciences, University of Iceland and the School of Earth and Environment, University of Leeds. Gas and PM filters were extracted following an established procedure (Ilyinskaya et al., 2021; Mason et al., 2021). All filters were cut into quarters and transferred to acid-cleaned 50 ml centrifuge tubes using acid-cleaned metal-free scissors and tweezers prior to the extraction process.

Gas filters were leached in 20 ml Milli-Q (>18.2 MOhm, MQ) water and 250 µl H_2O_2 (to oxidize collected sulfur species to sulfate) and then shaken for 20 min. 1.5 ml from these solutions was pipetted for anion concentration measurements by ion chromatography (IC) at the Department of Geography, University of Leeds (on Thermo Dionex ICS5000) and Institute of Earth Sciences, University of Iceland (on Thermo Dionex ICS2000).

Material collected on PM filters was extracted using a two-stage sequential leaching method (Ilyinskaya et al., 2021; Mason et al., 2021). The water-soluble PM fraction was first extracted in 20 ml MQ water +200 µl propan-2-ol (to reduce the hydrophobicity of the PM filters), shaken and placed in a sonic bath (20 min each), before being centrifuged at 3,000 rpm for 20 min. 10 ml of the solution was then pipetted to 15 ml acid-clean tubes for analysis by ICP-MS/MS (Agilent 8800), with another 1.5 ml pipetted for IC analysis (as described for the gas filters above). The remaining solution and filters were transferred to an acid-cleaned 22 ml PFA vial. 5 ml UPA grade concentrated HNO_3 was added to the PFA beaker and samples were dried on a hot plate at 55°C. 1 ml UPA grade concentrated HNO_3 and 1 ml UPA grade concentrated HF were pipetted to the solid residue and refluxed for 3 hr at 110°C with lids on the PFA beakers. The lids were then removed and the samples dried at 55°C. 10 ml UPA grade concentrated HNO_3 was then pipetted to the solid residue and refluxed on a hot plate at 90–100°C for 3 hr. Filters were then removed from the beakers using acid-cleaned metal-free tweezers and stored in original 50 ml centrifuge tubes. The solution was then dried down at 55°C and 0.5 ml UPA grade concentrated HNO_3 was pipetted to the final solid residue and refluxed at 90–100°C for 1 hr to get the sample back into solution. 10 ml MQ was pipetted into the PFA beakers and then transferred to an acid-cleaned sample tube for analysis by ICP-MS/MS.

PM filter samples and blanks were analyzed for major and trace elements by ICP-MS/MS in the School of Environment, Earth and Ecosystem Sciences at the Open University, UK. Field, lab, and filter blanks were used to quantify the level of contamination at all stages of the sampling and extraction process and were found to be negligible (see Figure S3 in Supporting Information S1 for blank comparison). Synthetic calibration standards were doped with the same solution matrix as samples in order to eliminate ionization effects (particularly with samples containing propan-2-ol). Ionization effects were monitored by running an on-line internal standard throughout all measurement sessions. Elements were analyzed using a triple quad set up with different collision gas modes (no gas, O_2, and NH_3) to minimize polyatomic and isobaric interferences. This allows for lower detection limits and improved accuracy across the range of elements analyzed.

Using ground mass major and trace element compositions from each of the three eruption years as representative silicate ash compositions (see Section 3.4 for details of groundmass analysis), a weighted ash fraction (WAF) calculation (Aiuppa et al., 2003) was also performed for filter pack trace element concentrations in this study. The WAF calculation assumes that the concentration of volatile element A on the filter is derived from two volcanic components - silicate ash and non-silicate aerosol - and was performed as a check on the relative contribution of silicate ash and dust to overall element concentrations on the filters (see Data Set S1 for full details of the calculation). Across all samples, the proportion of ash X_{ash} on the filter by weight was $<1 \times 10^{-3}$ (Table S1 in Supporting Information S1). Given the very small contribution of silicate ash, we use non-ash corrected element concentrations in the main body of this work to allow for inclusion of a greater array of trace elements. Figure S7 in Supporting Information S1 shows a comparison of non-ash-corrected and ash-corrected data with minimal differences in element concentrations across all samples.

3.3. Gas Composition Retrieved From FTIR Spectra

Selected gas ratios (SO_2/HCl, SO_2/HF, HCl/HF, mol/mol) and gas composition data (SO_2, HCl, HF, H_2O, CO_2, mol%) were obtained using open-path Fourier Transform Infrared FTIR spectra throughout the 2021 Fagradalsfjall eruption. Data included in this study were collected on 23rd March (vent measurements previously reported in Halldórsson et al. (2022) and 14th April 2021 (which are the most closely aligned with our aerosol samples) from within 300 m of vents 2, 3, and 5 (overview of measurements performed in Table 1, major gas data reported in Table 2). The open-path spectra were collected with a MIDAC FTIR spectrometer equipped with a liquid nitrogen-cooled mercury cadmium telluride (MCT) detector and 3-inch Newtonian telescope with a 10 mrad field of view. Interferograms and single beam spectra were collected at 0.5 cm^{-1} resolution approximately every 2 s. Examples of collected spectra from the same eruption on a different day are shown in Scott et al. (2023). The column amount of gases contributing to the measured spectra was determined using the Reference Forward Model (Dudhia, 2017) to simulate absorptions of target volcanic and atmospheric gas molecules in a specified spectral range using line parameters taken from the HITRAN database (Rothman et al., 1998). The model uses a two-layer atmosphere species reflecting a short path through a warm plume containing volcanic gas species and cooler ambient air for the rest of the path between the spectrometer and infrared source (Burton et al., 2007). The volcanic gas temperature was set between 450 and 400 K for the vent measurements and between 320 and 350 K for the lava flow measurements, using the temperature-dependent $\nu 1 + \nu 3$ feature at 2450–2550 cm^{-1} to estimate gas temperature (La Spina et al., 2015; Smekens et al., 2024). This temperature range reflects the rapid cooling of the volcanic gas as it mixed with the atmosphere. The calculations were conducted using the FTIR FIT software (Burton et al., 2007). The wavebands selected for retrieval were 2,020–2,150 (for CO_2, H_2O), 2,450–2,650 (SO_2), 2,600–3,100 (HCl), and 4,000–4,100 cm^{-1} (HF). Gas ratios (SO_2/HCl, SO_2/HF, and HCl/HF) were obtained for each measurement by averaging retrieved column amounts for a given data set (e.g., the mean and SD of SO_2 molecules cm^{-2} divided by HCl molecules cm^{-2}). To calculate gas composition (mol %), corrections for ambient air, H_2O, and CO_2 column amounts were performed by linear regression and subtracting the *y*-intercept from the retrieved column amounts. Gas ratios for at-vent and above flow measurements are reported in Table 2 and gas compositions, used for thermochemical modeling input, are reported in Sheet S6 in Data Set S1.

3.4. Groundmass Major and Trace Element Composition

Matrix glass samples from all three eruption years were analyzed for major and trace elements via JEOL JXA-8230 SuperProbe electron probe micro-analyzer (EPMA) at the Institute of Earth Sciences, University of Iceland and LA-ICP-MS/MS (Agilent 8800) at the Open University using analytical techniques outlined in Jenner and O'Neill (2012) for trace elements. Ag analysis was done by line scan on matrix glasses with the same approach as described in Wieser et al. (2020) for Se analysis in melt inclusions. The ZrO interference correction was done as described in Reekie et al. (2019), with reference material analyses for Ag from Jenner et al. (2015). These analyses were undertaken to determine the ash composition for each eruption (see Sheets S9 and S10 in Data Set S1).

3.5. Liquid-Only Thermometry

Liquid-only thermometry was performed using Thermobar (Wieser et al., 2022), using the major element concentrations from samples for all three eruption years (for details of major and trace element analysis see

Table 2
Overview of Gas Ratios Measured Using FTIR and MultiGAS At-Vent and Above Lava Flows

Date of measurement	Measurement type	Figure 2 ID	SO_2/HCl mol/mol	SO_2/HF mol/mol	H_2S/SO_2 mol/mol
FTIR—this study					
4/14/2021	Crater	5A	23.3	52.5	–
4/14/2021	Crater	5A	23.0	76.7	–
4/14/2021	Crater	5B	14.8	37.0	–
4/14/2021	Above flow	5B-L	12.6	32.2	–
4/14/2021	Above flow	5A-L	11.3	24.3	–
4/14/2021	Above flow	5AB-M	10.0	23.3	–
4/14/2021	Above flow	3-L	10.0	20.0	–
3/23/2021	Crater	B	75.0	125.0	–
3/23/2021	Crater	A	114.0	228.0	–
3/23/2021	Above flow	D	22.4	55.3	–
3/23/2021	Above flow	E	14.4	18.7	–
3/23/2021	Above flow	C	11.6	29.5	–
FTIR—Halldórsson et al. (2022)					
23/3/2021	Crater	–	65.3	261.0	–
25/3/2021	Crater	–	59.2	98.7	–
25/3/2021	Crater	–	67.8	169.5	–
25/3/2021	Crater	–	75.4	125.7	–
31/3/2021	Crater	–	30.9	72.0	–
31/3/2021	Crater	–	33.2	39.8	–
31/3/2021	Crater	–	31.9	55.8	–
5/4/2021	Crater	–	49.7	139.2	–
5/4/2021	Crater	–	45.4	63.6	–
5/4/2021	Crater	–	48.8	113.9	–
5/4/2021	Crater	–	51.6	137.7	–
MultiGAS—this study					
23/03/2021	Above flow	300 m from vent	–	–	0.15
13/04/2021	Crater	-	–	–	0.29
23/03/2021	Crater	-	–	–	0.00
16/08/2022	Crater	-	–	–	0.23
16/08/2022	Crater	-	–	–	0.19
19/07/2023	Above flow	250 m from vent	–	–	0.21

Note. Changes in SO_2/Halogen ratios down-flow are shown in Figure 2. Data from Halldórsson et al. (2022) is included for comparison between at-vent FTIR measurements. For both data sets SO_2/Halogen ratios fall within the same order of magnitude and show similar ranges between measurements. SO_2/HCl on the 14th April in notably lower than previous measurements (both in this study and in Halldórsson et al., 2022) reflecting the changing lava composition between Phase I and Phase II of the 2021 eruption. FTIR measurements reported in this study are split by sampling date and ordered by increasing distance from vent (all within ~300 m).

Supporting Information S1). Calculations were performed using Equations (15) and (22) from Putrika (2008), Equation (6a) from Sugawara (2000), and Helz and Thornber (1987). For the 2021 eruption, the calculated temperatures ranged from 1164°C to 1193°C, 1164°C to1185°C in 2022, and 1162°C to 1187°C in 2023 (±30°C, See Table S2 in Supporting Information S1). No liquid only thermometry has been calibrated specifically for Iceland and thus multiple globally calibrated thermometers were used to assess the sensitivity of calculated

temperatures to the chosen thermometer. Temperatures were consistent within error of one another across all samples and equations (See Table S2 in Supporting Information S1). The samples used were either airfall tephra or quenched lava samples collected close to the active fissure or vent and thus constrain a minimum eruptive temperature of 1180°C ± 30°C (used as the input for HSC thermochemical modeling below).

3.6. Thermochemical Modeling

The Gibbs free energy minimization (GEM) module of HSC chemistry (version 9.9.2, Outotec Research Oy, Finland) was used to model equilibrium gas phase element speciation in the lava flow emissions. Model inputs are major and trace species gas concentrations (kmol), pressure, temperature and the phases expected in the aerosol plume (see Symonds & Reed, 1993, Gerlach, 2004, Martin et al., 2006 for detailed description of the model and Mason et al., 2021, Mandon et al., 2019 for more recent applications). Trace element speciation in the aerosol emissions of a degassing lava flow was modeled under the following conditions: major gas concentrations (e.g., SO_2, CO_2, H_2O, H_2S, HCl, HF) were derived from FTIR measurements collected on 14th April 2021 (sample 5A for at-crater and sample 5AB-M for lava conditions in Figure 4), trace element concentrations from FP sample SFP3 (collected above lava flow) and SFP4 (collected at-crater), 1 bar pressure, and temperature range of 400–1200°C to investigate the temperature dependence of element speciation. See Sheet S7 in Data Set S1 for all input conditions and Sheet S8 in Data Set S1 for the full modeled output list of species expected in the plume.

Species modeled in this study are limited to the gas phase to investigate element speciation at the point of emission at the lava-air interface, and therefore the role of speciation behavior in the relative volatilization of different trace metals from lava flows as they cool and age down-flow. Gas phase-only modeling was also performed by Mason et al. (2021), and Mandon et al. (2019). As such, similarly limiting our modeling to the gas phase allows for comparison of metal and metalloid speciation between rift dominated (Fagradalsfjall, this study) hotspot (Hawai'i; Mason et al., 2021) and arc (Yasur, Mandon et al., 2019) settings, respectively.

Mason et al., 2021 previously investigated the effects of mixing with the atmosphere on element speciation behavior by increasing the amount of oxygen inputted into their model over a series of steps to account for an increasingly dilute plume. They found that once a "compositional discontinuity" (around 15 mol% air) was reached, the speciation behavior of certain elements may be altered (i.e., from a sulfide to a chloride). We choose not to include post-emission mixing with air in our modeling approach as the focus of this study is to investigate the relationship between the emission behavior of different elements in thermally and compositionally evolving flows and the speciation of those elements at the point at which they are emitted. The concentration of a given element measured on the filter is not affected by the speciation of that element when it is collected (i.e., Zn is measured as Zn irrespective of being ZnS or ZnCl). This means that post-emission changes in speciation (due to mixing with external air) do not affect our comparison between element speciation at emission (from modeling results) and relative behavior in down-flow emissions (collected via filter pack sampling. We do account for increased oxidation of the lava down-flow, however, by increasing the SO_2/H_2S ratio between vent and lava in our model inputs.

In Section 4.1, modeling is performed over the 400–1200°C temperature range, where the decrease in temperature reflects cooling of the lava (i.e., a lower emission source temperature) rather than the cooling of a single packet of gaseous plume due to mixing with ambient air. Modeling was performed down to the 400°C to account for the widest range of cooling of the lava flows. Nonetheless, crystallization of basaltic glass occurs in air at ~840°C (Burkhard, 2005) with the glass transition occurring at ~730°C (Ryan & Sammis, 1981). Below 700°C, the flows will therefore be almost completely solidified. Fractures in the lava flow may facilitate continued outgassing, although the magnitude of emissions from nearly solidified lava flows is likely to be much lower than from fully molten moving flows. The effect of this degree of cooling on the emission of trace elements remains uncertain, for example, the extent to which trace elements can diffuse through the remaining melt and be outgassed from nearly solidified lava flows.

4. Results

4.1. At-Vent and Down-Flow Degassing of Major Gas Species

As shown in Figure 2, FTIR measurements, from both crater and lava flow emissions, reveal a decrease in SO_2/halogen gas ratios with increasing distance from the crater during the 2021 eruption. These measurements were

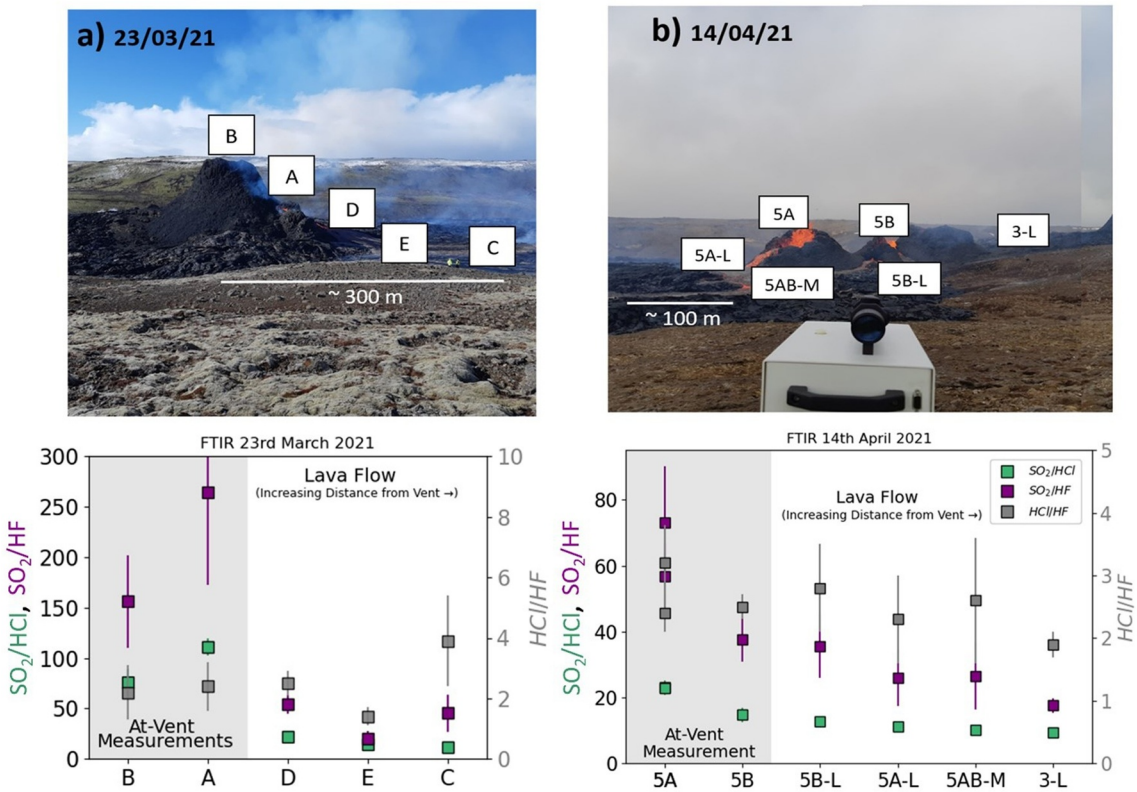

Figure 2. FTIR measurements collected within 300 m of source at-vent and adjacent lava flow locations during the 2021 eruption. Panel (a) shows annotated photograph of vent 2 (23/03/21). Panel (b) shows annotated photographs of vent 5 (14/04/21). Panels (c) and (d) show SO_2/halogen gas ratios in mol/mol, with lava flow measurements ordered on the *x*-axis by increasing the distance from vent. Green squares show SO_2/HCl ratios and purple squares show SO_2/HF, both of which are lower in lava flow measurements compared to main vent degassing and decrease as lava flow distance from the active vent increases.

performed at two active craters and several down-flow locations close to the active craters, as detailed in annotations on Figure 2 and Sheet S4 in Data Set S1). In Figure 2, measurements from degassing lava flows are ordered by increasing distance from their respective vents, although there was some potential mixing between lava flows from the multiple craters that were active in close proximity during sampling. For both data sets, SO_2/HCl and SO_2/HF molar ratios are higher at-vent compared to lava flow measurements (see Table 2). On 23rd March 2021, the average at-vent SO_2/HCl ratio was 93 ± 18 mol/mol, whilst the average SO_2/HF ratio was 216 ± 50 mol/mol. On 14th April, these ratios were significantly lower, with an average SO_2/HCl of 20 ± 4 mol/mol and SO_2/HF of 55 ± 18 mol/mol. Both data sets show a decrease in SO_2/halogen ratios along flow, with the most distal SO_2/HCl and SO_2/HF ratios decreasing to ~10 mol/mol and ~20 mol/mol, respectively. Figure 2 shows that HCl/HF also decreases with increasing distance from the vent (gray squares), suggesting a relative increase in HF outgassing in the more distal lava flows. Since all FTIR measurements were collected above relatively young lava flows within 300 m of an active vent, it remains unclear to what extent SO_2/halogen ratios would continue to decrease (if at all) in older and more evolved flows.

4.2. Trace Element Emissions

During ICP-MS analysis, 57 elements were measured above detection limits on PM filter samples. At-crater concentrations ranged from $>1 \times 10^{-5}$ g/m^3 for elements such as Mg, Ca, K, Al, Na, Fe, and Se, between 1×10^{-5} and 1×10^{-7} g/m^3 for Ba, Ti, Mn, Ni, Cu, Zn, As, Sn, Pb, Cd, Te, and Ge, and $<1 \times 10^{-7}$ g/m^3 for Li, Cr, Co, Sb, Cs, Tl, Ag, and the REE (Sheet S3 in Data Set S1). Element concentrations in samples collected above outgassing lavas $[X]_{lava}$ were normalized to element concentrations in at-crater samples $[X]_{at\text{-}crater}$ to compare relative down-flow depletion in trace element emissions between samples and eruption years. Trace elements showed a range of relative depletion rates and behaviors (as discussed further in Section 4.2 below. Te, Se, As, Pb, and Sn consistently showed the highest relative depletion in lava outgassing compared to at-crater emissions, with

concentrations in the most distal lava FP samples being up to three orders of magnitude lower than in at-vent emissions. More moderate rates of down-flow depletion are shown by other elements, including Mn, Cu, Rb, Cs, as well as Ag, Zn, and Cd, which are up to one order of magnitude less abundant in down-flow emissions compared to at-vent element concentrations. La, Ce, Mg, Fe, Ti, and Al show the lowest relative rates of depletion down-flow, with comparable element concentrations between at-vent and lava flow emissions.

5. Discussion

We now explore further the behavior of selected elements, considered representative of the range of element volatilities and speciation behaviors, through thermochemical modeling and discuss our observations in the context of the degassing behavior of major gases (SO_2, HCl, HF). We propose a mechanism where element speciation plays a dominant role in controlling the down-flow fractionation in trace element emissions from outgassing lava flows, where the speciation behavior of some elements is dependent on the age and thermal evolution of the lava.

5.1. Trace Element Speciation Under Lava Flow Conditions

As lava flows are exposed to ambient surface temperatures, they undergo cooling and crystallization. Using at-crater major gas and trace element input conditions (outlined in Section 3.6 and Sheet 7 in Data Set S1), element equilibrium speciation was modeled across the 1200°C–400°C temperature range to simulate post-eruptive cooling of the lava (Cashman et al., 1999) and investigate subsequent changes in element speciation due to decreasing lava temperature (Figure 3). Liquid thermometry constraints from quenched lava and tephra samples provided a minimum eruptive temperature of 1180°C ± 30°C. As shown in Figure 3, at this temperature, with at-vent major gas and trace element input conditions, the resultant groups of gaseous complexes are: sulfides (Se, Te, As, Pb, Sn), chlorides (Cs, Rb, Cu, Ce), hydroxides (Mn, Fe, Al, Ti, Mg), oxides (La), and elemental forms (Ag, Zn, Cd). Nonetheless, uncertainties in trace element and major gas input conditions are reflected in the thermochemical modeling output, particularly the temperatures at which speciation transitions occur. The sensitivities of modeled speciation behavior to major gas and trace element input conditions are investigated below; however, the temperature dependent speciation transitions modeled here should be considered as approximate constraints on transition temperatures.

As shown in Figure 3, the refractory elements Ti and Al complex predominantly as hydroxides across the whole temperature range. By contrast, Fe and Mg complex as hydroxides at higher temperatures but transition to predominant chloride species under lower temperature conditions. La and Ce transition from oxide to chloride complexing behavior with decreasing temperature, with a further transition at lower temperatures to include an additional fluoride component. Similar chloride-to-fluoride transition is also seen for elements Cs, Al, Mg, and Rb with decreasing temperatures. Cu remains complexed as a chloride across the whole modeled temperature range. Only three elements, Ag, Cd, and Zn, show elemental speciation behavior, although all have a greater chloride component at lower temperatures. The remaining elements, Pb, Sn, As, Se, and Te predominantly complex as sulfides across the modeled temperature range, although Pb and Sn show a transition to chloride-complexing behavior at lower temperatures. By contrast, As shows a higher temperature transition with increasing oxide component under higher temperature conditions.

In addition to cooling, lava flow gas emissions also undergo compositional changes as they age due to crystallization and associated enrichment of incompatible elements in the residual melts. This includes decreasing SO_2/halogen ratios with increasing distance from the crater (shown with FTIR measurements in Figure 2) as well as becoming increasingly oxidized as the lava reacts with air down-flow (Lerner et al., 2021). Multi-GAS measurements were used to constrain approximate SO_2/H_2S ratios (where SO_2/H_2S reflects the ratio between the oxidized species SO_2 and the more reduced species H_2S) for at-vent and lava flow emissions. At-vent emissions had a lower SO_2/H_2S ratio ∼6.6 and whilst emissions sampled above the lava had a higher SO_2/H_2S ratio of ∼12.1 reflecting increased oxidation down flow (see Sheet S5 in Data Set S1). To account for variations in gas composition, thermochemical speciation modeling was repeated at 1180°C under both at-crater (higher SO_2/HCl, lower SO_2/H_2S) and lava flow (lower SO_2/HCl, higher SO_2/H_2S) gas input conditions. Trace element inputs from at-crater (SFP4) and lava (SFP3) filter pack samples were also used to account for down-flow changes in element chemistry. The minimum temperature input was set to 1180°C ± 30°C based on liquid thermometry constraints

10.1029/2024GC011822

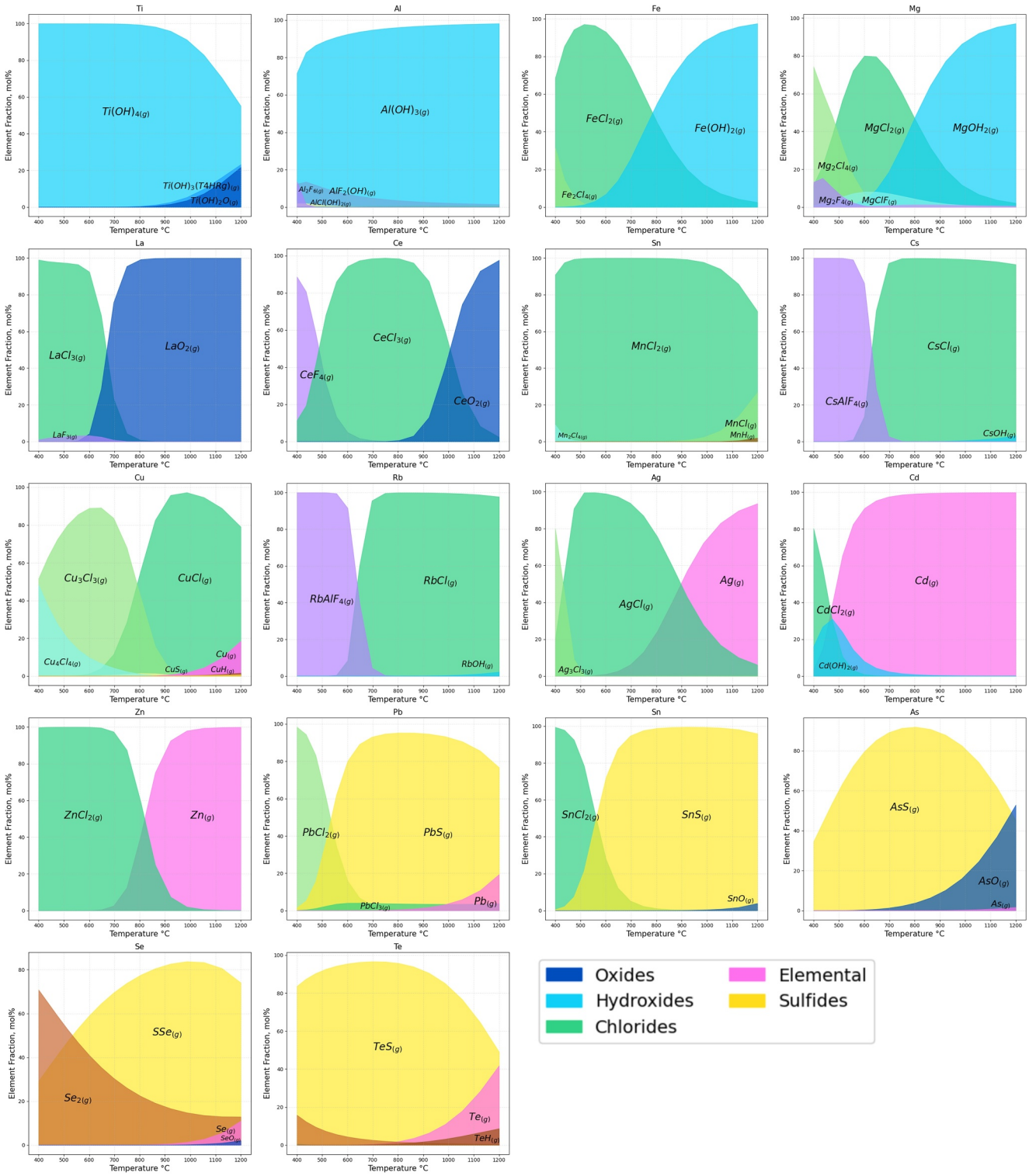

Figure 3. Equilibrium element speciation modeling between 400°C and 1200°C. Input trace element and major gas compositions are from the 2021 at-crater FP sample (SFP4) and FTIR vent measurements, input conditions are outlined in full in Sheet S7 (Data Set S1).

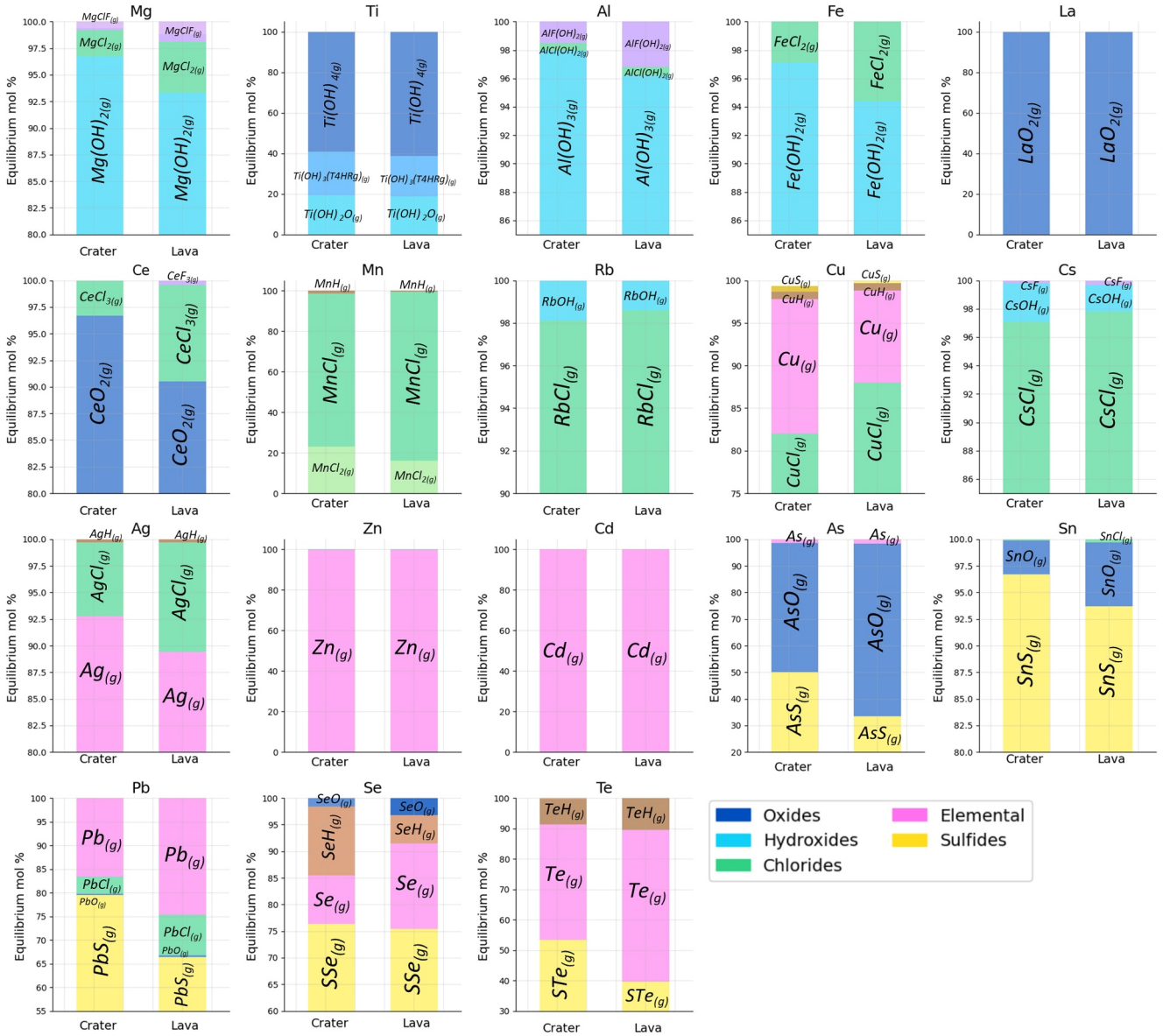

Figure 4. Element Speciation at 1180°C (based on liquid thermometry temperature constraints) under at-crater and lava flow conditions. Input SO_2/HCl ratios were constrained from FTIR (SO_2/HCl_{crater} = 23 mol/mol, SO_2/HCl_{lava} = 11.3 mol/mol), and input SO_2/H_2S from MultiGAS data ($H_2S/SO_{2crater}$ = 0.29 mol/mol, H_2S/SO_{2lava} = 0.15 mol/mol). Modeling was performed using the Gibbs free energy minimization module of HSC Chemistry. Trace element and concentration inputs from lava flow filter pack (SFP3) and at-crater filter pack (SFP4) from 2021 eruption.

and held constant across both crater and lava inputs to deconvolve the effects of decreasing lava temperature (modeled above) from the effects of changing composition.

As shown in Figure 4, speciation groupings (by mol%) are broadly similar under both at-crater and lava flow conditions at 1180°C. Only elements As and Te show a difference in their speciation behaviors; complexing dominantly sulfides under at-vent conditions to predominantly complexing as oxides (As) and elementally (Te), respectively, under lava flow conditions. Minor changes in speciation behavior are also observed for Mg, Fe, Ce, Rb, Ag, and Pb in the form of a small increase (<10%) in the proportion of chloride-complexed species under lava flow trace element and major gas input conditions. This shift from sulfide to chloride speciation most likely reflects the decreasing availability of the S^{2-} ligand (lost to degassing) and relative increase in the availability of the Cl^- ligand as the lava evolves compositionally down-flow, which is reflected in the decreasing SO_2/HCl ratio with distance from vent (Figure 2). Several elements, such as Mg, Al, and Ce, also have a slightly greater fluoride

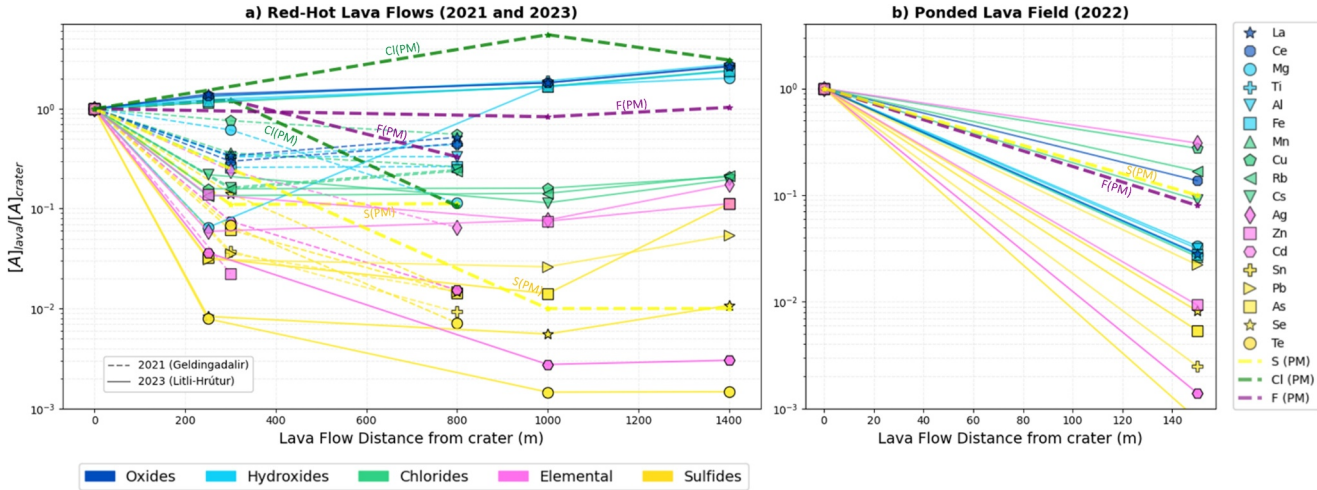

Figure 5. Trace element emission evolution along degassing lava flows at the 2021, 2022, and 2023 Fagradalsfjall eruptions. (a) Geldingadalir 2021 eruption and Litli-Hrútur 2023 eruption. (b) Meradalir 2022 eruption, Y-axis shows the lava flow $[A]_{lava}$ concentration (ug/m^3 air pumped) normalized to the source concentration $[A]_{crater}$ at discrete distances sampled along the lava flow ranging from 200 m to 1.4 km (3 samples in 2021, 2 in 2022, and 4 in 2023). The concentrations shown in this figure are non-ash corrected in order to include the more refractory elements such as Fe, Mg, and Ti, although the ash corrected version is shown in Figure S5 in Supporting Information S1. The proportion of ash on the filters X_{ash} is $<1 \times 10^{-3}$ across all samples used in this study and thus, as shown in Figure S5 in Supporting Information S1, the ash correction has negligible impact on element concentrations. Lava flows in 2021 and 2023 were extending laterally and thus relative distance from vent also reflects relative flow age within each sampling year. The down-flow sample in 2022 was collected above a degassing vent within a ponded lava field, and thus the close distance to vent is not necessarily representative of a younger sample age. Element coloring in this figure reflects major speciation behavior modeled for lava flow conditions at 1180°C, where yellow are the S-complexing elements, pink the elemental, green Cl-complexing, and blue the hydroxide and oxide complexing elements (see Figure 4).

component when modeled using lava flow compositional inputs (trace elements and gases), although overall the proportion of fluoride-complexed species for these elements remains minor relative to the chloride and oxide-complexed component. The increased prevalence of a fluoride complexed component also likely reflects a relative increase in the availability of the F^- ligand with increasing distance down-flow, shown by decreasing HCl/HF with increasing distance from vent (Figure 2). Further compositional changes in older, more evolved lava flows than captured by our measurements and modeling may drive continued progression toward increasing chloride and fluoride speciation.

Overall, the speciation behaviors identified here in the Fagradalsfjall emissions (both under lava and at-crater conditions) are consistent with previous modeling work for the Fissure 8 plume during the Kīlauea 2018 eruption (Hawai'i), with nearly identical complexing behavior across the array of trace elements common to both studies (Mason et al., 2021). Given the similarities in plume chemistry between the Fagradalsfjall 2021 and Kīlauea 2018 eruptions, it is therefore expected that these similar input chemistries would result in similar model output speciation results Nonetheless, differences in element speciation behavior are seen when compared to modeling performed with inputs from arc setting volcanoes. For example, Zn and Pb show elemental and sulfide speciation, respectively, in both the Fagradalsfjall and Kīlauea plumes, but predominantly show chloride speciation in similar modeling work for the Yasur volcanic plume (Mandon et al., 2019). We propose this difference can be explained based on the relative availability of S^{2-} and Cl^- ligands. High SO_2/HCl mass ratios were measured in gas emissions from Fagradalsfjall in 2021 (25–40; this study) and Kīlauea 2018 (32–35; Mason et al., 2021), reflecting the absence of a Cl-rich recycled slab component seen at subduction zone volcanoes such as Yasur (SO_2/HCl mass ratio = 5.6–12.8; Mandon et al., 2019), where the Cl^- ligand is more abundant. Together, this difference in speciation and gas composition highlights the importance of the S2- ligand for metal transport in rift-dominated settings, as has already been identified at hotspot basaltic volcanoes such as Kīlauea (Mason et al., 2021).

5.2. Down-Flow Evolution of Trace Element Emissions

Figure 5 shows element concentrations in FP samples collected above outgassing lava flows at different distances from the crater, normalized to at-crater element concentrations. Data sets have been grouped by those collected

above laterally extending, visibly flowing, red-hot lava (Panel a—all samples in 2021 and 2023) and those collected above a single vent in a ponded, stagnant lava field (Panel b; 2022). See Figure S3 in Supporting Information S1 for examples of lava flow conditions.

Across all three eruptions, the sulfur-complexing elements (as defined by modeling in Section 4.1) Se, Te, As, Pb, and Sn (shown in yellow) deplete more rapidly relative to chloride (green), elemental (pink) and oxide/hydroxide (blue) complexing elements with increasing distance from the source crater. For emissions above red-hot lava flows, sulfur-complexing elements are up three orders of magnitude lower in concentration than in at-vent emissions within 1 km down-flow, whilst the concentrations of chloride complexing elements are only one order of magnitude less than in crater emissions at the same distance. For samples collected above the ponded lava field in 2022, the sulfur-complexing elements show a similar degree of depletion to those samples at ∼1 km distance in 2023 despite being much more proximal to the vent. The relative behavior of chloride-, oxide-, and hydroxide-complexing elements, however, shows a greater dependence on lava flow style. For example, chloride-complexing elements Mn, Cu, Rb, and Cs show a relative depletion compared to refractory elements in 2021 and 2023 emissions (above red-hot lava flows) but a relative enrichment compared to the same refectory elements in 2022 where the lava field was ponded. The refractory elements (e.g., La, Ce, Mg, Fe, Ti, Al, shown in blue, Figure 5) show minimal down-flow depletion above the red-hot lava flows in 2021 and 2023, but are depleted by up to an order of magnitude in emissions sampled above the ponded lava vent in 2022.

An overall down-flow fractionation between S and Cl can be seen both in the behavior of sulfur and chloride-complexing elements in filter pack samples (Figure 5) and in the decreasing SO_2/halogen ratios with increasing distance down-flow (Figure 2) observed in FTIR measurements. Filter pack samples collected during the Holuhraun 2014–2015 eruption showed a reduction in S/Cl and S/F ratios from the syn-eruptive gas plume (analogous to our at-vent samples) to the post-eruptive gas phase (lava flow), which was explained by Rayleigh distillation and decreasing availability of S in the crystallizing magma (Sigmarsson et al., 2020). Aiuppa (2009) similarly concludes that lower SO_2/HCl and SO_2/HF ratios are characteristic of the late stages of volcanic degassing, where the higher melt solubilities of the halogens mean they are less likely to enter the gas phase relative to S. Observations of SO_2 and HCl gas fluxes during the 2008–2009 eruption of Mt Etna and adjacent periods of quiescence suggest that halogen degassing is driven by prolonged shallow crystallization, whilst S is lost more rapidly from the melt (La Spina et al., 2023).

Toutain et al. (1990) observed a similar fractionation in S-Cl and S-F specifically in degassing lava flows on Piton de la Fornaise, with an absence of sulfides or sulfates further down-flow, leaving sublimates instead dominated by chloride and fluoride species. This can be seen in Figure 5 (denoted by bolder dashed lines), where S(PM) decreases much more rapidly in down-flow emissions relative to Cl(PM) and F(PM) in both 2021 and 2023 samples. The more rapid depletion of sulfur-complexing elements down-flow compared to other complexes most likely reflects earlier upstream sulfur degassing where the rapid volatilization and emission of sulfur-complexing elements close to the vent leaves them in low abundances in the silicate melt with little left to degas down-flow. Both FTIR and trace element concentrations show the highest rate of depletion in S and sulfur-complexing elements within a few hundred meters of the vent, with the rate of depletion then plateauing in the more distal lava flow samples. However, the higher solubilities of Cl and F in the silicate melt mean that their degassing is delayed and they remain in greater abundance in the down-flow region (following the accepted sequence of volatile solubility S < Cl < F in basaltic melt; Carroll & Webster, 1994). Consequently, chloride- and fluoride-complexing elements continue to degas even in the most distal regions of lava flows. Sigmarsson et al. (2020) and Toutain et al. (1990) also report a decrease in HCl/HF with increasing distance down flow, which is similarly seen in our FTIR data (in Figure 2). Nonetheless, there is no indication of a coincident increase in the volatilization and emission of fluoride-complexing elements (such as Al, Cs, Ce, Rb) in the most distal regions down-flow. This can be explained by speciation modeling under a more evolved lava flow composition (Figure 4), which shows that although the relative importance of fluoride complexes does increase compared to main vent emissions, fluorides still remain a minor component compared to chlorides and hydroxides in overall element complexing behavior. Even with an increase in F degassing down-flow the impact on trace element emissions would therefore still be limited. The limited role of F degassing may reflect the young ages of the lava flows that were sampled, and so under more evolved lava flow conditions (older and more degassed), it is possible that relatively greater emission of fluoride complexing elements such as Ce, Al, Rb, and Cs could be observed with increasing distance down-flow.

Toutain et al. (1990) previously identified a down-flow fractionation in trace elements based on element relative volatility, rather than speciation, where volatile elements such as Rb, Cs, Se, Pb, and Tl were detected in low-temperature deposits, but refractory elements (such as Fe, Mg, Ti, Ce) were not detected. This result was attributed to the refractory elements not being volatized down-flow at lower temperatures. Figure S6 (Supporting Information S1) shows Figure 5 with elements colored by emanation coefficient rather than speciation behavior (description of emanation coefficient calculation in Supporting Information S1, and coefficients included in Sheet S13 in Data Set S1). Element emission behavior down-flow shows a strong correlation with element emanation coefficients, although this is unsurprising given the strong link between speciation and volatility (i.e., sulfides and chlorides are relatively more volatile than oxides and hydroxides). The effects of the volatility fractionation can also be seen in the filter pack sample from 2022 (ponded lava field), where the relative depletion in down-flow emissions between chloride and oxide/hydroxide elements is reversed relative to samples in 2021 and 2023 (see Figure 5), with the chloride group of elements showing relative enrichment compared to oxide/hydroxide elements in 2022. Sample collection in 2021 and 2023 occurred above red-hot lava flowing laterally away from the vent, whereas the 2022 sample was collected above an isolated degassing vent that had been present within the ponded lava field for at least 3 days, with no incandescent lava visible. The 2022 sample therefore likely represents degassing from the oldest and most evolved lava flow across the three eruptions that we sampled. As the lava flow cools, the extent to which the most refractory elements (e.g., Fe, Mg, Ti, La) are able to be volatilized decreases, whilst the more volatile halogen gases (and F- and Cl-complexed elements with them) continue to be volatized to a greater extent at lower temperatures (volatility fractionation; identified in Toutain et al., 1990). Nonetheless, volatility alone cannot explain element behavior in 2022. Elements Ce, Ag, Cu, Rb, and Cs all show similar rates of depletion in downflow emissions; however, they have a wide range of emanation coefficients (Ce being the most refractory; $\varepsilon = 3.2E\text{-}05$, and Ag being the most volatile; $\varepsilon = 0.5$). Instead the commonality across that group of elements is their speciation behavior and predominantly complexing as chloride species (as shown by modeling in Figures 3 and 4 above).

As shown in Figure 5, Ce and Ag also show notably variable behavior across the different eruption years, which have varied lava flow styles. In 2021 and 2023 (red-hot lava flows), Ce behaves similarly to the other oxide/hydroxide-complexed elements, whilst in 2022 ponded lava flow emissions, Ce tracks more closely with chloride complexing elements such as Rb and Cs. Considering the temperature dependence shown by Ce speciation behavior (Figure 3), this potentially reflects a transition from Ce complexing as an oxide to chloride being the dominant species as the lava flow cools. When modeled under lava flow rather than crater conditions (Figure 4), the relative importance of chloride/fluoride speciation also increases for Ce, and thus the later volatilization of Cl and F may further contribute to increased emission of Ce in an older and compositionally more evolved flow. Ag also shows variable depletion depending on lava flow style, behaving similarly to the elementally complexed Zn in 2021 and 2023, but then tracking much more closely with the chloride complexing elements Cu and Rb above the ponded lava field in 2022. As with Ce, Ag also undergoes a speciation transition towards a more dominant chloride component at lower temperatures (see equilibrium speciation modeling in Figure 3). Given that the vent within the ponded lava field had been present for several days and did not show visibly incandescent lava, it is reasonable that this sample represents emissions from a colder and more degassed lava. Lava flow age can therefore be linked to the thermal evolution and composition of gas emissions, which, as shown by thermochemical modeling, are both key controls on trace element speciation and emission behavior in outgassing lava flows.

Overall, several transitions in lava outgassing composition are observed within our Fagradalsfjall data set. These are outlined schematically in Figure 6 and include: (a) predominant degassing of SO_2 and sulfur-complexing elements at-vent; (b) a rapid drop off in S emissions as lava flows age and cool, leaving more distal emissions governed by chloride and oxide/hydroxide degassing; (c) continued cooling means the volatilization of refractory elements also decreases, leaving the most evolved lava flow outgassing dominated by Cl-gases and volatile chloride-complexed elements. (d) increasing F/Cl ratios down-flow (also observed by Toutain et al., 1990; Sigmarsson et al., 2020) suggest there is the potential that even colder and more evolved lava flow emissions may be dominated by the outgassing of fluoride-complexed elements (such as Rb, Mg, Al Cs, and Ce at lower temperatures).

The compositional evolution of lava flow emissions from the S-dominated degassing near-vent to an increasingly Cl- and F-dominated regime down-flow, has implications for different trace metal exposure hazard, which we suggest may vary depending on lava flow age and thermal evolution. Emissions from the youngest lava flows are

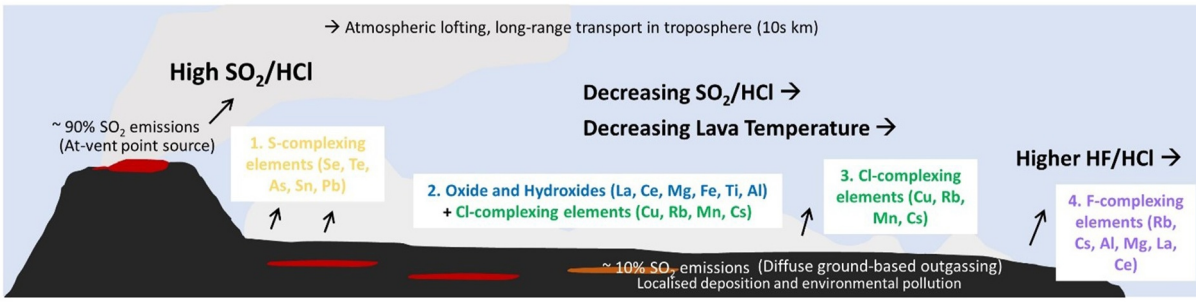

Figure 6. Schematic diagram of the observed and modeled transitions in the gas and trace element composition of lava flow outgassing emissions. Phases 1, 2, and 3 were observed in trace element and major gas behavior in this study. At-vent emissions were also dominated by Phase 1. Phase 4 was inferred from speciation modeling and increasing HF/HCl ratios down-flow (supported by similar observations in Toutain et al., 1990; Sigmarsson et al., 2020). 90% of total volcanic SO_2 was emitted at the vent, as calculated below based on lava degassing data from Pfeffer et al. (2024). Atmospheric lofting and long-range transport of elements (up to 50 km) in the main vent plume were reported by Ilyinskaya et al. (2021) for the 2018 Kīlauea eruption (Hawai'i).

likely dominated by trace metals such as Se, Sn, Te, Pb, and As, whilst further down-flow the emission trace metal profile is dominated by elements such as Cs, Rb, Cu, Zn, and Ce.

5.3. Trace Element Fluxes

The relative fluxes of trace elements from lava flows are more poorly constrained compared to at-vent emissions, and yet could have important implications for understanding the potential contribution of lava flow outgassing to overall volcanic emissions, environmental loading, and air quality impacts. Trace element fluxes cannot be measured directly but can be estimated by combining element X/SO_2 ratios with independent measurements of SO_2 flux:

$$X_{flux} = SO_{2flux} * \frac{X}{SO_2}. \quad (1)$$

where X_{flux} and SO_{2flux} are the flux of element X and SO_2, respectively, and X/SO_2 is the concentration ratio of element X and SO_2 derived from filter pack and Multi-GAS measurements. SO_2 fluxes were taken from DOAS traverse measurements during the 2021 eruption (Pfeffer et al., 2024) across the two periods most closely aligned with our sampling dates (i.e., the 21/03 and 24/03 span the time window in which our sampling on the 23/03 took place). The minimum and maximum SO_2 fluxes were used to calculate upper and lower bound estimates for trace element emission fluxes and were between 11–99 kg/s SO_2 flux between 21st and 24th March 2021, and between 21–97 kg/s SO_2 flux between 13th and 17th April 2021 (from Pfeffer et al., 2024).

Groundmass glass (GG) and melt inclusion (MI) data reported in Pfeffer et al. (2024) were used to estimate the relative proportions of at-vent and lava flow degassing in 2021, assuming that total volcanic SO_2 flux is derived predominantly from at-vent degassing but with an additional lava outgassing component. MI and GG data are from quenched lava and air fall tephra samples collected during the 2021 eruption (see Pfeffer et al., 2024 for full methodology). To calculate the relative proportion of at-vent outgassing, we use a bulk approach which subtracts the average S content of tephra groundmass glass (120 ppm) from the average S content of the undegassed melt inclusions (960 ppm) divided by the average S content of the undegassed melt inclusions (960 ppm) to get an at-vent degassing proportion of 88% (±2%—1SD). The relative proportion of lava flow degassing was then approximated by subtracting the minimum S content of lava sample groundmass glass (40 ppm) from the average S content of the tephra groundmass glass (120 ppm) and divided by the average S content of the undegassed melt inclusions (960 ppm). This constrains a relative lava degassing proportion of ~8% (±4%—1SD), although it does not account for the effects of fractional crystallization down-flow. The proportion of total degassing comprised of vent and lava sources was therefore taken forward as 90% vent degassing and 10% lava outgassing when calculating the relative emissions of trace elements from vent and lava below.

The calculated emission rates of selected volatile and potentially toxic trace metals (Cr, Ni, Cu, As, Se, Pb, and Cd) from volcanic sources during the 2021 Fagradalsfjall eruption are comparable to or greater than equivalent annual average anthropogenic emissions in Iceland during 2021 (Figure 7; black bars). The elements shown in

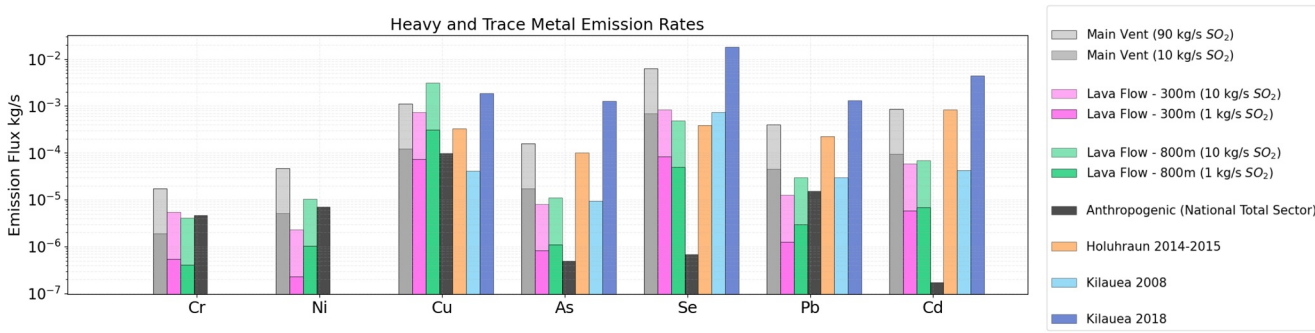

Figure 7. Emission flux estimates from volcanic sources at the Fagradalsfjall 2021 eruption and anthropogenic emissions in Iceland 2021 (Environment Agency of Iceland, 2023). Volcanic emissions are divided into main vent and lava flow estimates, where, based on petrological estimates, lava flow emissions account for ~10% of total SO_2 flux. Trace element fluxes were calculated by combining independent DOAS SO_2 flux estimates and [X]/[SO_2] ratios from filter pack samples SFP3 (300 m) and SFP8 (800 m)—[X]/[SO_2] data reported in Sheet S11 in Data Set S1. Also shown is a comparison of Icelandic volcanic emission fluxes with fluxes from other global basaltic eruptions. Holuhraun 2014–2015 data from Gauthier et al. (2016). Kilauea 2008 and 2018 data from Ilyinskaya et al. (2021). X/SO_2 and emission flux data for a wider selection of elements and gases are included in Sheet S11 in Data Set S1.

Figure 7 were chosen as they are identified as metal pollutants in Iceland (Environment Agency of Iceland, 2023). Across all seven elements, main vent volcanic emission fluxes (gray bars) were estimated using both upper (90 kg/s SO_2) and lower (10 kg/s SO_2) SO_2 fluxes. During the period of active eruptive activity, the emission rates (in kg/s) of several elements, such as Cr, Ni, Cu, and Pb, in the main vent volcanic are comparable in magnitude to anthropogenic emissions, whilst for elements (As, Se, and Cd), volcanic emissions are two to three orders of magnitude greater than those from anthropogenic sources during the 2021 eruption.

Trace element fluxes from lava flows were also calculated using 10% of the total volcanic SO_2 flux (from DOAS) at both an upper (10 kg/s) and lower estimate (1 kg/s). These lava flow SO_2 fluxes were then combined with element [X]/[SO_2] ratios from one proximal vent (SFP3—300 m) and one more distal (SFP8—800 m) FP sample to estimate element emission rates. Lava flow emissions of Cr, Ni, and Pb are up to an order of magnitude lower than main vent and anthropogenic emissions for the lower bound SO_2 flux but remain comparable in magnitude under higher SO_2 fluxes. For elements such as As, Se, and Cd, lava flow emissions remain up to two orders of magnitude greater than anthropogenic fluxes, even with the lower SO_2 flux estimate. However, fluxes remain lower than emissions from the main volcanic vent.

The exception to these observations is Cu, where the estimated flux from the most distal lava flow sample exceeds those from both the main vent and the more proximal lava flow sample. The higher [Cu]/[SO_2] ratio most likely reflects the more prolonged degassing of chlorides (as Cu predominantly complexes with Cl) relative to sulfide degassing down-flow. The effects of element speciation behavior and the transition toward a more chloride dominated degassing profile in more evolved lavas can similarly be seen in Ni, Pb, and Cd, where the more distal lava flow has a higher estimated emission flux of these elements for a given SO_2 flux. Nonetheless, SO_2 degassing does rapidly drop off as lava flows evolve further from the vent. Therefore, whilst lava flow emission fluxes have been calculated using the same upper and lower SO_2 bounds, the more distal lava flow likely sits at the lower end of the estimated SO_2 fluxes, whereas the more proximal sample is closer to the upper bound SO_2 flux. As such, although greater for a given SO_2 flux, the actual down-flow trace element emission of Cl-complexing elements in more distal lava flows may not exceed that of the more proximal lava flow emissions. By contrast, the sulfur-complexing elements (Se, Cd, As) show either greater trace element emission fluxes in the more proximal lava flow sample or a much smaller difference between the proximal and distal samples. The percentage decrease in element emissions was calculated between the more proximal (300 m from vent, upper bound of 10 kg/s SO_2) and more distal (800 m from vent, lower bound of 1 kg/s SO_2) lava flows for 2021 (Sheet 12 in Data Set S1). Between 300 and 800 m from the vent, element fluxes decreased to a highly variable extent, between 5% (Nd) and almost 100% (Zn, Ca, Mo). The sulfur-complexing elements such as Se, Te, Cd, and As showed some of the greatest decrease in emissions (between 94% and 86% decrease), whilst chloride complexing elements such as Cu, Rb, and Cs decreased to a lesser extent (between 13%–58%). Fractionation in element emissions is therefore occurring proximally to the vent, with the rapid reduction in sulfur-complexing elements (~90% reduction) occurring between 300 and 800 m, whilst the reduction in chloride complexing element fluxes occurs more gradually, with emissions of these elements persisting further down-flow.

Compared to anthropogenic activity, which generally leads to continuous emission output, emissions from volcanic activity cease or are greatly reduced during periods of quiescence. Assessing the significance of volcanic emissions within Iceland compared with anthropogenic emissions therefore requires consideration of the time-frame over which emissions are being released. Volcanic sources are most significant over timescales of eruptive activity, which are typically weeks or months depending on the eruption. Volcanic activity on the Reykjanes Peninsula has become more frequent over the past 4 years, with eight eruptions occurring between March 2021 and March 2024. The relative importance of volcanic emissions to the atmosphere, on both a regional and national scale, has therefore increased. Compared to global anthropogenic emissions of trace metals, Icelandic national sector emissions are however relatively low, with global fluxes being dominated by China, India, Russia, and the US (Zhu et al., 2020). Emission fluxes from the Fagradalsfjall 2021 eruption were comparable to those from the Kīlauea 2008 (Ilyinskaya et al., 2021) and Holuhraun 2014–2015 eruptions (Gauthier et al., 2016) although much lower than emission fluxes calculated for the Kīlauea 2018 eruption (Ilyinskaya et al., 2021).

During the 2018 Kīlauea eruption (Hawai'i) and 2021 Tajogaite eruption (Cumbre Vieja, La Palma), lava flows progressed toward, and reached, populated areas. Emissions from outgassing lava flows therefore potentially increased population exposure to volcanic pollutants even when the main plume from the volcanic vent was not grounding in that area (BBC News, 2021; National Park Service, 2021). Compared to emissions from the main volcanic vent, which are generally concentrated from a single point source, emissions from degassing lava flows occur dispersed over a much greater area and so are more dilute as well as less thermally buoyant than the main vent plume. Trace elements emitted from degassing lava flows are therefore more likely to be concentrated at ground-level and dispersed more locally (10 s m) than those emitted in the main vent plume (10 s km—see Ilyinskaya et al., 2021). Whilst this study focused on relatively young lava flows which degassed during ongoing periods of eruptive activity, lava flows may continue to degas for weeks and months following an eruption and thus present a prolonged risk to air quality and environmental exposure to heavy metals (Simmons et al., 2017). The most recent Sundhnúkur 2023–2024 eruptions on the Reykjanes peninsula have also occurred with much higher initial effusion rates (over 1200 m^3/s in the first few hours) and in closer proximity to people working (including the workers building the lava barriers which has even included scraping cooled lava to be used as fill material in the barriers) compared to the Fagradalsfjall 2021–2023 eruptions. The ongoing frequency at which eruptions are now occurring on the peninsula (weeks-months), leading to repeated emission of fresh lava flows, means there is greater potential for localized environmental metal pollution (e.g., in hydrological reservoirs).

6. Conclusions

Using UAS-mounted samplers, we collected particulate matter (PM) and gas samples above outgassing lava flows at increasing distances from the source during the Fagradalsfjall 2021–2023 eruptions. We find that the composition of emissions from degassing lava flows evolves as the flow ages and cools:

- Near-vent emissions have high SO_2/halogen ratios and are dominated by the outgassing of S-complexing trace elements such as Se, Te, Pb, As, and Sn, where speciation groupings were defined from thermochemical modeling.
- S degassing rapidly decreases as lava flows age and cool, accompanied by progressively reducing SO_2/halogen ratios. Outgassing is dominated by chloride (Cs, Cu, Mn, Rb), oxide (Ce, La), and hydroxide (Mg, Ti, Fe, Al) complexed elements.
- Decreasing lava temperatures result in reduced volatilization of the most refractory elements as well as resulting in a transition in speciation behavior in some elements, such as Ag and Ce. The most distal lava flow emissions are therefore dominated by Cl degassing and Cl-complexed elements.
- According to our modeling and previous measurements, the most evolved (oldest, coolest) lava flows transition further to being dominated by fluoride degassing, with increasing F/Cl ratios down-flow and increased emission of fluoride-complexed elements (Rb, Cs, Al) as inferred from speciation modeling. This remains a hypothesis to be tested for these recent Icelandic eruptions.

Overall, these results evidence that the hazard posed by trace metal emissions, particularly in terms of potential public exposure, is not constant and instead depends strongly on lava age and thermal evolution. Estimated fluxes of volatile trace metals from degassing lava flows were shown to be only an order of magnitude less than those from main vent degassing and for a selection of environmentally polluting elements greater than or equal to anthropogenic fluxes in Iceland. This finding highlights the importance of considering lava flow outgassing in

total volcanic emissions budgets for basaltic eruptions, where their contribution may have previously been disregarded. The Sundhnúkur 2023–2024 eruptions, which remain ongoing at the time of writing, continue to impact the environment. Protracted degassing from the regular and voluminous lava flows leads to localized contamination by metal pollutants, which is particularly hazardous given the proximity of flow emplacement to substantial population centers on the Reykjanes peninsula.

Conflict of Interest

The authors declare no conflicts of interest relevant to this study.

Data Availability Statement

The gas and trace element data presented in this study and used in subsequent modeling calculations are available from the CEDA Archive via https://catalogue.ceda.ac.uk/uuid/f29f666e890045c783b4eef7399e9cc5/ with a creative commons license, no registration required (Wainman et al., 2024). Data is also included in Data Set S1.

Acknowledgments

Laura Wainman acknowledges that this work was supported by the Leeds–York–Hull Natural Environment Research Council (NERC) Doctoral Training Partnership (DTP) Panorama (Grant NE/S007458/1). Evgenia Ilyinskaya also acknowledges support from Centre for Observation and Modeling of Earthquakes, Volcanoes and Tectonics (COMET) and NERC Urgency Grant NE/Z000262/1 "Chemistry of emissions at lava-urban interfaces". Analysis costs were also partially covered by the Icelandic Research Fund (RANNÍS): Magma dynamics on the Reykjanes Peninsula (MaDre)—Integrated geochemical and geophysical investigation of the (on-going) 2021 Fagradalsfjall eruption (Grant 228933-053). Josefa Sepúlveda-Araya thanks the National Agency for Research and Development (ANID) for the support with the Scholarship program, Beca de Doctorado en el Extranjero 72210412. Adam Cotterill acknowledges support from the London NERC DTP and Brock Edwards from the Geological Survey of Canada (Environmental Geosciences Program) and the Natural Sciences and Engineering Research Council of Canada. We also thank Claire Horwell for kindly lending equipment to support our field campaigns, and the pilots at Svarmi for their incredible drone flying across many field campaigns.

References

Aiuppa, A. (2009). Degassing of halogens from basaltic volcanism: Insights from volcanic gas observations. *Chemical Geology*, *263*(1–4), 99–109. https://doi.org/10.1016/j.chemgeo.2008.08.022

Aiuppa, A., Dongarrà, G., Valenza, M., Federico, C., & Pecoraino, G. (2003). Degassing of trace volatile metals during the 2001 eruption of Etna. In A. Robock & C. Oppenheimer (Eds.), *Volcanism and the Earth's atmosphere geophysical monograph 139* (pp. 41–54). American Geophysical Union.

Aiuppa, A., Federico, C., Giudice, G., & Gurrieri, S. (2005). Chemical mapping of a fumarolic field: La Fossa crater, Vulcano Island (Aeolian Islands, Italy). *Geophysical Research Letters*, *32*(13), L13309. https://doi.org/10.1029/2005gl023207

Allard, P., Aiuppa, A., Bani, P., Métrich, N., Bertagnini, A., Gauthier, P.-J., et al. (2016). Prodigious emission rates and magma degassing budget of major, trace and radioactive volatile species from Ambrym basaltic volcano, Vanuatu island Arc. *Journal of Volcanology and Geothermal Research*, *322*, 119–143. https://doi.org/10.1016/j.jvolgeores.2015.10.004

Barsotti, S., Parks, M., Pfeffer, M. A., Óladóttir, B. A., Barnie, T., Titos, M., et al. (2023). The Eruption in Fagradalsfjall (2021, Iceland): How the operational monitoring and the volcanic hazard assessment contributed to its safe access. *Natural Hazards*, *116*. https://doi.org/10.21203/rs.3.rs-1453832/v1

BBC News. (2021). *Canary Islands: Lava from erupting volcano destroys homes*. BBC News. Retrieved from https://www.bbc.co.uk/news/world-europe-58620555#:~:text=A%20volcano%20eruption%20on%20La

Burkhard, D. J. M. (2005). Relation between oxidation/crystallization and degassing upon reheating of basalt glass from Kilauea, Hawaii. *Mineralogical Magazine*, *69*(2), 103–117. https://doi.org/10.1180/0026461056920238

Burton, M., Aiuppa, A., Allard, P., Asensio-Ramos, M., Cofrades, A. P., La Spina, A., et al. (2023). Exceptional eruptive CO_2 emissions from intra-plate alkaline magmatism in the Canary volcanic archipelago. *Communications Earth & Environment*, *4*(1), 467. https://doi.org/10.1038/s43247-023-01103-x

Burton, M., Allard, P., Muré, F., & La Spina, A. (2007). Magmatic gas composition reveals the source depth of slug-driven strombolian explosive activity. *Science*, *317*(5835), 227–230. https://doi.org/10.1126/science.1141900Caracciolo

Carroll, M. R., & Webster, J. D. (1994). Solubilities of sulfur, noble gases, nitrogen, chlorine, and fluorine in magmas. *Reviews in Mineralogy and Geochemistry*, *30*(1), 231–279.

Cashman, K. V., Thornber, C., & Kauahikaua, J. P. (1999). Cooling and crystallization of lava in open channels, and the transition of Pāhoehoe Lava to 'A'ā. *Bulletin of Volcanology*, *61*(5), 306–323. https://doi.org/10.1007/s004450050299

Churakov, S. V., Tkachenko, S. I., Korzhinskii, Bocharnikov, R. E., & Shmulovich, K. I. (2000). Evolution of composition of high-temperature fumarolic gases from Kudryavy Volcano, Iturup, Kuril Islands: The thermodynamic modeling. *Geochemistry International*, *38*(5).

Dudhia, A. (2017). The reference forward model (RFM). *Journal of Quantitative Spectroscopy and Radiative Transfer*, *186*, 243–253. https://doi.org/10.1016/j.jqsrt.2016.06.018

Edmonds, M., Mather, T. A., & Liu, E. J. (2018). A distinct metal fingerprint in arc volcanic emissions. *Nature Geoscience*, *11*(10), 790–794. https://doi.org/10.1038/s41561-018-0214-5

Edwards, B. A., Pfeffer, M. A., Ilyinskaya, E., Kleine-Marshall, B. I., Mandon, C. L., Cotterill, A., et al. (2024). Exceptionally low mercury concentrations and fluxes from the 2021 and 2022 eruptions of Fagradalsfjall volcano, Iceland. *Science of the Total Environment*, *917*, 170457. https://doi.org/10.1016/j.scitotenv.2024.170457

Einarsson, S., & Sigurgeirsson, M. A. (2019). Reykjanes-Svartsengi. In B. Oladottir, G. Larsen, & M. T. Guðmundsson (Eds.), *Catalogue of Icelandic volcanoes*. IMO, UI and CPD-NCIP. Retrieved from http://icelandicvolcanoes.is/?volcano=REY#

Environment Agency of Iceland. (2023). Informative inventory report emissions of air pollutants in Iceland from 1990 to 2021. Retrieved from https://www.ust.is/library/Skrar/loft/IIR/IIR%202023.pdf

Gauthier, P.-J., Sigmarsson, O., Gouhier, M., Haddadi, B., & Moune, S. (2016). Elevated gas flux and trace metal degassing from the 2014-2015 fissure eruption at the Bárðarbunga volcanic system, Iceland. *Journal of Geophysical Research: Solid Earth*, *121*(3), 1610–1630. https://doi.org/10.1002/2015jb012111

Gerlach, T. M. (2004). Volcanic sources of tropospheric ozone-depleting trace gases. *Geochemistry, Geophysics, Geosystems*, *5*(9). https://doi.org/10.1029/2004gc000747

Global Volcanism Program. (2023). Report on Fagradalsfjall (Iceland). In S. Sennert (Ed.), *Weekly volcanic activity report, 2 August-8 August 2023*. Smithsonian Institution and US Geological Survey. Retrieved from https://volcano.si.edu/showreport.cfm?wvar=GVP.WVAR20230802-371032

Gunnarson, S. R., Belart, J. M. C., Óskarsson, B. V., Gudmundsson, M. T., Högnadóttir, T., Pedersen, G., et al. (2023). *Automated processing of aerial imagery for geohazards monitoring: Results from Fagradalsfjall eruption, SW Iceland, August 2022*. Zenodo (CERN European Organization for Nuclear Research). https://doi.org/10.5281/zenodo.7871187

Halldórsson, S. A., Marshall, E. W., Caracciolo, A., Matthews, S., Bali, E., Rasmussen, M. B., et al. (2022). Rapid shifting of a deep magmatic source at Fagradalsfjall volcano, Iceland. *Nature*, *609*(7927), 529–534. https://doi.org/10.1038/s41586-022-04981-x

Helz, R. T., & Thornber, C. R. (1987). Geothermometry of Kilauea Iki lava lake, Hawaii. *Bulletin of Volcanology*, *49*(5), 651–668. https://doi.org/10.1007/bf01080357

Hinkley, T. K., Marie-Françoise, L. C., & Lambert, G. (1994). Fractionation of families of major, minor, and trace metals across the melt-vapor interface in volcanic exhalations. *Geochimica et Cosmochimica Acta*, *58*(15), 3255–3263. https://doi.org/10.1016/0016-7037(94)90053-1

Ilyinskaya, E., Mason, E., Wieser, P. E., Holland, L., Liu, E. J., Mather, T. A., et al. (2021). Rapid metal pollutant deposition from the volcanic plume of Kīlauea, Hawai'i. *Communications Earth & Environment*, *2*(1), 1–15. https://doi.org/10.1038/s43247-021-00146-2

Ilyinskaya, E., Schmidt, A., Mather, T. A., Pope, F. D., Witham, C., Baxter, P., et al. (2017). Understanding the environmental impacts of large fissure eruptions: Aerosol and gas emissions from the 2014–2015 Holuhraun eruption (Iceland). *Earth and Planetary Science Letters*, *472*, 309–322. https://doi.org/10.1016/j.epsl.2017.05.025

Jenner, F. E., Hauri, E. H., Bullock, E. S., König, S., Arculus, R. J., Mavrogenes, J. A., et al. (2015). The competing effects of sulfide saturation versus degassing on the behavior of the chalcophile elements during the differentiation of hydrous melts. *Geochemistry, Geophysics, Geosystems*, *16*(5), 1490–1507. https://doi.org/10.1002/2014gc005670

Jenner, F. E., & O'Neill, H. S. C. (2012). Analysis of 60 elements in 616 ocean floor basaltic glasses. *Geochemistry, Geophysics, Geosystems*, *13*(2), Q02005. https://doi.org/10.1029/2011gc004009

La Spina, A., Burton, M., Salerno, G., & Caltabiano, T. (2023). Insights into magma dynamics at Etna (Sicily) from SO_2 and HCl fluxes during the 2008–2009 eruption. *Geology*, *51*(5), 419–423. https://doi.org/10.1130/g50707.1

La Spina, A., Burton, M. G., Allard, P., Alparone, S., & Murè, F. (2015). Open-path FTIR spectroscopy of magma degassing processes during eight lava fountains on Mount Etna. *Earth and Planetary Science Letters*, *413*, 123–134. https://doi.org/10.1016/j.epsl.2014.12.038

Lerner, A. H., Wallace, P. J., Shea, T., Mourey, A. J., Kelly, P. J., Nadeau, P. A., et al. (2021). The petrologic and degassing behavior of sulfur and other magmatic volatiles from the 2018 eruption of Kīlauea, Hawai'i: Melt concentrations, magma storage depths, and magma recycling. *Bulletin of Volcanology*, *83*(6), 43. https://doi.org/10.1007/s00445-021-01459-y

Liu, E. J., Aiuppa, A., Alan, A., Arellano, S., Bitetto, M., Bobrowski, N., et al. (2020). Aerial strategies advance volcanic gas measurements at inaccessible, strongly degassing volcanoes. *Science Advances*, *6*(44), eabb9103. https://doi.org/10.1126/sciadv.abb9103

Mandon, C. L., Christenson, B. W., Schipper, C. I., Seward, T. M., & Garaebiti, E. (2019). Metal transport in volcanic plumes: A case study at White Island and Yasur volcanoes. *Journal of Volcanology and Geothermal Research*, *369*, 155–171. https://doi.org/10.1016/j.jvolgeores.2018.11.024

Martin, R. S., Mather, T. A., & Pyle, D. M. (2006). High-temperature mixtures of magmatic and atmospheric gases. *Geochemistry, Geophysics, Geosystems*, *7*(4), Q04006. https://doi.org/10.1029/2005gc001186

Mason, E., Wieser, P. E., Liu, E. J., Edmonds, M., Ilyinskaya, E., Whitty, R. C. W., et al. (2021). Volatile metal emissions from volcanic degassing and lava–seawater interactions at Kīlauea Volcano, Hawai'i. *Communications Earth & Environment*, *2*(1), 1–16. https://doi.org/10.1038/s43247-021-00145-3

Mather, T. A., Witt, M. L. I., Pyle, D. M., Quayle, B. M., Aiuppa, A., Bagnato, E., et al. (2012). Halogens and trace metal emissions from the ongoing 2008 summit eruption of Kīlauea volcano, Hawai`i. *Geochimica et Cosmochimica Acta*, *83*, 292–323. https://doi.org/10.1016/j.gca.2011.11.029

Moune, S., Gauthier, P. J., & Delmelle, P. (2010). Trace elements in the particulate phase of the plume of Masaya Volcano, Nicaragua. *Journal of Volcanology and Geothermal Research*, *193*(3–4), 232–244. https://doi.org/10.1016/j.jvolgeores.2010.04.004

Moune, S., Gauthier, P.-J., Gislason, S. R., & Sigmarsson, O. (2006). Trace element degassing and enrichment in the eruptive plume of the 2000 eruption of Hekla volcano, Iceland. *Geochimica et Cosmochimica Acta*, *70*(2), 461–479. https://doi.org/10.1016/j.gca.2005.09.011

National Park Service. (2021). *2018 eruption and summit collapse - Hawai'i volcanoes national park*. U.S. National Park Service. Retrieved from https://www.nps.gov/havo/learn/nature/2018-eruption.htm#:~:text=In%202018%2C%20a%20new%20eruption

Pedersen, G. B. M., Belart, J. M. C., Óskarsson, B. V., Gudmundsson, M. T., Gies, N., Högnadóttir, T., et al. (2022). Volume, effusion rate, and lava transport during the 2021 Fagradalsfjall Eruption: Results from near real-time photogrammetric monitoring. *Geophysical Research Letters*, *49*(13), e2021GL097125. https://doi.org/10.1029/2021gl097125

Pennisi, M., Le Cloarec, M. F., Lambert, G., & Le Roulley, J. C. (1988). Fractionation of metals in volcanic emissions. *Earth and Planetary Science Letters*, *88*(3–4), 284–288. https://doi.org/10.1016/0012-821x(88)90085-4

Pfeffer, M. A., Arellano, S., Barsotti, S., Petersen, G. N., Barnie, T., Ilyinskaya, E., et al. (2024). SO_2 emission rates and incorporation into the air pollution dispersion forecast during the 2021 eruption of Fagradalsfjall, Iceland. *Journal of Volcanology and Geothermal Research*, *449*, 108064. https://doi.org/10.1016/j.jvolgeores.2024.108064

Putirka, K. D. (2008). Thermometers and barometers for volcanic systems. *Reviews in Mineralogy and Geochemistry*, *69*(1), 61–120. https://doi.org/10.2138/rmg.2008.69.3

Reekie, C. D. J., Jenner, F. E., Smythe, D. J., Hauri, E. H., Bullock, E. S., & Williams, H. M. (2019). Sulfide resorption during crustal ascent and degassing of oceanic plateau basalts. *Nature Communications*, *10*(1), 82. https://doi.org/10.1038/s41467-018-08001-3

Rothman, L. S., Rinsland, C. P., Goldman, A., Massie, S. T., Edwards, D. P., Flaud, J.-M., et al. (1998). The hitran molecular spectroscopic database and Hawks (hitran atmospheric workstation): 1996 edition. *Journal of Quantitative Spectroscopy and Radiative Transfer*, *60*(5), 665–710. https://doi.org/10.1016/s0022-4073(98)00078-8

Rubin, K. (1997). Degassing of metals and metalloids from erupting seamount and mid-ocean ridge volcanoes: Observations and predictions. *Geochimica et Cosmochimica Acta*, *61*(17), 3525–3542. https://doi.org/10.1016/s0016-7037(97)00179-8

Ryan, M. P., & Sammis, C. G. (1981). The glass transition in basalt. *Journal of Geophysical Research*, *86*(B10), 9519–9535. https://doi.org/10.1029/jb086ib10p09519

Scott, S., Pfeffer, M., Oppenheimer, C., Bali, E., Lamb, O. D., Barnie, T., et al. (2023). Near-surface magma flow instability drives cyclic lava fountaining at Fagradalsfjall, Iceland. *Nature Communications*, *14*(1), 6810. https://doi.org/10.1038/s41467-023-42569-9

Sigmarsson, O., Moune, S., & Gauthier, P. J. (2020). Fractional degassing of S, Cl and F from basalt magma in the Bárðarbunga rift zone, Iceland. *Bulletin of Volcanology*, *82*(7), 54. https://doi.org/10.1007/s00445-020-01391-7

Sigmundsson, F., Parks, M., Hooper, A., Geirsson, H., Vogfjörd, K. S., Drouin, V., et al. (2022). Deformation and seismicity decline before the 2021 Fagradalsfjall eruption. *Nature*, *609*(7927), 523–528. https://doi.org/10.1038/s41586-022-05083-4

Simmons, I. C., Pfeffer, M. A., Calder, E. S., Galle, B., Arellano, S., Coppola, D., & Barsotti, S. (2017). Extended SO_2 outgassing from the 2014–2015 Holuhraun lava flow field, Iceland. *Bulletin of Volcanology*, *79*(11), 79. https://doi.org/10.1007/s00445-017-1160-6

Smekens, J.-F., Mather, T. A., Burton, M. R., Varnam, M., & Pfeffer, M. A. (2024). Rapid primary sulfate aerosol generation observed with OP-FTIR in the eruptive plume of the Fagradalsfjall basaltic eruption, Iceland, 2021. *Journal of Geophysical Research: Atmospheres*, *129*(12), e2023JD040574. https://doi.org/10.1029/2023JD040574

Stewart, C., Damby, D. E., Horwell, C. J., Elias, T., Ilyinskaya, E., Tomašek, I., et al. (2021). Volcanic air pollution and human health: Recent advances and future directions. *Bulletin of Volcanology*, *84*(1), 11. https://doi.org/10.1007/s00445-021-01513-9

Sugawara, T. (2000). Empirical relationships between temperature, pressure, and MgO content in olivine and pyroxene saturated liquid. *Journal of Geophysical Research*, *105*(B4), 8457–8472. https://doi.org/10.1029/2000jb900010

Symonds, R. B., & Reed, M. H. (1993). Calculation of multicomponent chemical equilibria in gas-solid-liquid systems; calculation methods, thermochemical data, and applications to studies of high-temperature volcanic gases with examples from Mount St. Helens. *American Journal of Science*, *293*(8), 758–864. https://doi.org/10.2475/ajs.293.8.758

Symonds, R. B., Reed, M. H., & Rose, W. I. (1992). Origin, speciation, and fluxes of trace-element gases at Augustine volcano, Alaska: Insights into magma degassing and fumarolic processes. *Geochimica et Cosmochimica Acta*, *56*(2), 633–657. https://doi.org/10.1016/0016-7037(92)90087-y

Symonds, R. B., Rose, W. I., Reed, M. H., Lichte, F. E., & Finnegan, D. L. (1987). Volatilization, transport and sublimation of metallic and non-metallic elements in high temperature gases at Merapi Volcano, Indonesia. *Geochimica et Cosmochimica Acta*, *51*(8), 2083–2101. https://doi.org/10.1016/0016-7037(87)90258-4

Thordarson, T., & Self, S. (2003). Atmospheric and environmental effects of the 1783–1784 Laki eruption: A review and reassessment. *Journal of Geophysical Research*, *108*(D1), AAC7-1–AAC7-29. https://doi.org/10.1029/2001jd002042

Toutain, J. P., Aloupogiannis, P., Delorme, H., Person, A., Blanc, P., & Robaye, G. (1990). Vapor deposition of trace elements from degassed basaltic lava, Piton de la Fournaise volcano, Reunion Island. *Journal of Volcanology and Geothermal Research*, *40*(3), 257–268. https://doi.org/10.1016/0377-0273(90)90124-x

Wainman, L., Ilyinskaya, E., Pfeffer, M., Scott, S. W., Mandon, C., Bali, E., et al. (2024). *Lava aerosol gas and trace element data from the Fagradalsfjall 2021-2023 eruption, Iceland*. NERC EDS Centre for Environmental Data Analysis. https://doi.org/10.5285/f29f666e890045c783b4eef7399e9cc5

Wieser, P., Petrelli, M., Lubbers, J., Wieser, E., Ozaydin, S., Kent, A., & Till, C. (2022). Thermobar: An open-source Python3 tool for thermobarometry and hygrometry. *Volcanica*, *5*(2), 349–384. https://doi.org/10.30909/vol.05.02.349384

Wieser, P. E., Jenner, F., Edmonds, M., Maclennan, J., & Kunz, B. E. (2020). Chalcophile elements track the fate of sulfur at Kīlauea Volcano, Hawai'i. *Geochimica et Cosmochimica Acta*, *282*, 245–275. https://doi.org/10.1016/j.gca.2020.05.018

Williams-Jones, A. E., & Heinrich, C. A. (2005). 100th anniversary special paper: Vapor transport of metals and the formation of magmatic-hydrothermal ore deposits. *Economic Geology*, *100*(7), 1287–1312. https://doi.org/10.2113/gsecongeo.100.7.1287

World Health Organisation. (2007). *Health risks of heavy metals from long-range transboundary air pollution (EUR/06/5067592)*. WHO Regional Office for Europe.

Zelenski, M., Simakin, A. V., Taran, Y. V., Sebastien, M., & Malik, N. S. (2021). Partitioning of elements between high-temperature, low-density aqueous fluid and silicate melt as derived from volcanic gas geochemistry. *Geochimica et Cosmochimica Acta*, *295*, 112–134. https://doi.org/10.1016/j.gca.2020.12.011

Zelenski, M. E., Fischer, T. P., de Moor, J. M., Marty, B., Zimmermann, L., Ayalew, D., et al. (2013). Trace elements in the gas emissions from the Erta Ale volcano, Afar, Ethiopia. *Chemical Geology*, *357*, 95–116. https://doi.org/10.1016/j.chemgeo.2013.08.022

Zhu, C., Tian, H., & Hao, J. (2020). Global anthropogenic atmospheric emission inventory of twelve typical hazardous trace elements, 1995–2012. *Atmospheric Environment*, *220*, 117061. https://doi.org/10.1016/j.atmosenv.2019.117061

Zoller, W. H., Parrington, J. R., & Kotra, J. M. P. (1983). Iridium enrichment in airborne particles from Kīlauea Volcano: January 1983. *Science*, *222*(4628), 1118–1121. https://doi.org/10.1126/science.222.4628.1118